

THIRD ORDER OPTICAL NONLINEARITIES

Mansoor Sheik-Bahae

Department of Physics and Astronomy
University of New Mexico,
Albuquerque, NM 87131

Michael P. Hasselbeck

Department of Physics and Astronomy
University of New Mexico,
Albuquerque, NM 87131

| | | |
|--------------|---|-----------|
| I. | INTRODUCTION..... | 2 |
| II. | QUANTUM MECHANICAL PICTURE..... | 4 |
| III. | NONLINEAR ABSORPTION (NLA) AND NONLINEAR REFRACTION (NLR) | 6 |
| IV. | KRAMERS-KRONIG DISPERSION RELATIONS..... | 8 |
| V. | OPTICAL KERR EFFECT | 11 |
| | • BOUND ELECTRONIC OPTICAL KERR EFFECT IN SOLIDS..... | 11 |
| | • RE-ORIENTATIONAL KERR EFFECT IN LIQUIDS | 12 |
| VI. | THIRD-HARMONIC GENERATION | 13 |
| VII. | STIMULATED SCATTERING | 13 |
| | • STIMULATED RAMAN SCATTERING | 14 |
| | • STIMULATED BRILLOUIN SCATTERING | 16 |
| VIII. | TWO PHOTON ABSORPTION | 17 |
| IX. | EFFECTIVE THIRD-ORDER NONLINEARITIES; CASCADED $\chi^1:\chi^1$ PROCESSES | 18 |
| | • OPTICALLY GENERATED PLASMAS | 19 |
| | • ABSORPTION SATURATION | 19 |
| | • THERMAL EFFECTS | 20 |
| | • PHOTOREFRACTION | 21 |
| X. | EFFECTIVE THIRD-ORDER NONLINEARITIES; CASCADED $\chi^{(2)}:\chi^{(2)}$ PROCESSES..... | 21 |
| XI. | PROPAGATION EFFECTS..... | 22 |
| | • SELF-FOCUSING | 23 |
| | • SOLITONS..... | 23 |
| XII. | COMMON EXPERIMENTAL TECHNIQUES AND APPLICATIONS | 24 |
| | • TIME RESOLVED EXCITE-PROBE TECHNIQUES | 25 |
| | • FOUR-WAVE MIXING..... | 26 |
| | • INTERFEROMETRY | 27 |
| | • Z-SCAN..... | 27 |
| | • ALL-OPTICAL SWITCHING AND OPTICAL BISTABILITY | 28 |
| XIII. | REFERENCES..... | 29 |
| XIV. | FIGURE CAPTIONS | 36 |

I. Introduction

The subject of this chapter could well fill a textbook and indeed, comprises a significant portion of the many books on nonlinear optics. A large, but by no means exhaustive or complete list of texts that provide extensive discussion of high-order nonlinearities is as follows [1-30]. We have not attempted to write a review article nor mentioned or even listed every known third-order nonlinear optical phenomenon. Our aim is to illustrate important and representative third-order effects, emphasizing qualitative descriptions. Details can be found in the references. An exception is our discussion of the Kramers-Kronig relations in nonlinear optics. A fundamental premise of this transformation is the causal link between nonlinear refraction and nonlinear absorption, which is a key aspect of the third-order susceptibility. It has not been treated in most texts; some of the important mathematical steps are given here. Our treatment of third-order nonlinear optics assumes the reader is familiar with electromagnetic theory, physical optics, and quantum mechanical energy level diagrams.

Any real, physical oscillating system will exhibit a nonlinear response when it is overdriven. In an optical system, a nonlinear response can occur when there is sufficiently intense illumination. The nonlinearity is exhibited in the polarization (P) of the material, which is often represented by a power series expansion of the total applied optical field (E):

$$P = \epsilon_0 \chi^{(1)} E + \epsilon_0 \chi^{(2)} E^2 + \epsilon_0 \chi^{(3)} E^3 + \dots \quad (1)$$

Here $\chi^{(1)}$ is the linear susceptibility representing the linear response (i.e. linear absorption and the refractive index) of the material. The two lowest order nonlinear responses are accounted for by the second and third order nonlinear susceptibilities $\chi^{(2)}$ and $\chi^{(3)}$. The subject of this chapter is third-order effects. Processes arising from the second-order response (including second-harmonic generation and optical parametric processes) are discussed elsewhere in this handbook series [Chapter 38, Ebrahimzadeh's chapter]. We will, however, briefly consider the cascading of second order nonlinearities that appear as an "effective" third order process in section X.

Third order optical nonlinearities cover a vast and diverse area in nonlinear optics. A simple illustration of this point is the reported range of magnitudes and response times for $\chi^{(3)}$ in various materials, which span 15 orders of magnitude! This has led to unavoidable inconsistency and confusion in the definition and interpretation of the nonlinear susceptibility. We will not be immune from such inconsistencies and errors. In that spirit, we note that the simple, power series representation of the nonlinear optical response described by Eq. (1) is not rigorously correct because it assumes the response is instantaneous. In the case of the bound-electronic nonlinearity for example, this assumption is excellent because the response is exceedingly fast. The response is not *infinitely* fast, however. Response times can vary by orders of magnitude depending on the physical mechanism and resonance conditions involved. Furthermore, Eq.(1) assumes locality, which implies the nonlinear polarization at a given point in space depends on the magnitude of the electric field only at that point. This condition is not always satisfied. The electrostrictive nonlinearity, for example, is the result of physical displacement of charged particles in a material subject to the ponder-motive force due to the gradient of light irradiance. It is therefore non-local. It is nevertheless instructive to apply Eq.(1) to describe various third-order effects that are local and (single photon) non-resonant.

The nonlinear polarization represented in Eq. (1) excludes "effective" third-order nonlinear processes involving linear absorption ($\chi^{(1)}$ process) of one of the excitation beams. An example is the thermal nonlinearity resulting from linear absorption and heating that causes a change of

refractive index. Although this is effectively a third-order nonlinear response, we group this and similar phenomena in Section IX on cascaded $\chi^{(1)}:\chi^{(1)}$ effects .

The term involving E^{-3} in Eq.(1) implies that three optical fields interact to produce a fourth field. The $\chi^{(3)}$ interaction is thus a four-photon process. This is a consequence of the quantum mechanical picture of the nonlinear susceptibility. Conservation of photon energy is always required to complete the interaction process. Assuming the applied optical fields are monochromatic plane waves, we write the total input electric field E^- as:

$$E^-(r, t) = E_1^-(r, t) + E_2^-(r, t) + E_3^-(r, t) \quad (2)$$

In general, each beam has a different frequency (ω) and wave vector (\vec{k}), represented in complex notation:

$$E_j^-(r, t) = \frac{\vec{E}_j}{2} \exp(i\omega_j t - i\vec{k}_j \cdot r) + c.c. \quad \text{for } j=1,2,3 \quad (3)$$

where c.c. stands for complex conjugate and \vec{E}_j is a complex vector describing the amplitude, phase, and polarization of each beam. It is important to realize that there can be up to three different input laser frequencies, but there can be as few as one. Ignoring the $\chi^{(1)}$ and $\chi^{(2)}$ components in Eq.(1), the nonlinear polarization resulting from the E^{-3} interaction leads to a total of 108 terms involving all possible permutations of the fields at three frequencies. The nonlinear polarization occurs at frequencies given by:

$$\omega_4 = \pm\omega_i \pm \omega_j \pm \omega_k \quad \text{for } i,j,k=1,2,3. \quad (4)$$

The existence of 108 terms does not mean there are as many distinct mechanisms involved. For instance, three terms give $\omega_4=3\omega_j$, for $j=1,2,3$, describing exactly the same process of third-harmonic generation (THG). Furthermore, THG is a special case of sum frequency generation (SFG) involving one, two, or three different frequencies giving $\omega_4=\omega_i+\omega_j+\omega_k$, $i,j,k=1,2,3$ accounting for 27 terms.

One realizes 108 permutations with different time ordering of three different laser beams distinguished by frequency, and/or wave vector, and/or polarization. If only two distinguishable laser beams are available, the number of permutations decreases to 48. When the system is driven by a single beam, the third-order response involves only four terms in three fields. In general, the $\chi^{(3)}$ coefficients associated with each term will be different due to the ever-present dispersion (i.e. frequency dependence) of the susceptibilities. The frequency dependence is a direct consequence of the finite response time of the interaction. We will expand on this subject in the discussion of the Kramers-Kronig dispersion relations in section IV.

Another important property of nonlinear susceptibilities is their tensor nature. Because of the molecular or lattice structure of materials, the nonlinear response will depend on the state of the polarization of the optical fields. For the sake of brevity, we neglect the tensor properties of $\chi^{(3)}$ and treat all the susceptibilities and electric fields as scalar quantities. The reader may consult textbooks on nonlinear optics for detailed discussions of this subject.

Propagation of interacting beams is also an important consideration and one must account for wavevector summation (i.e. conservation of momentum) that results from the E^{-3} operation. It is useful to invoke the four photon picture, recalling that the momentum of each photon is given by $\hbar\vec{k}_j$. Taking the resultant nonlinear polarization to be a plane wave with a wavevector \vec{k}_4 ,

momentum conservation requires that:

$$\vec{k}_4 = \pm \vec{k}_i \pm \vec{k}_j \pm \vec{k}_k \quad (5)$$

where $|\vec{k}_j| = n(\omega_j)\omega_j/c$. This phase-matching requirement is not necessarily satisfied in every interaction due to dispersion of the linear refractive index in the material. Phase matching can be a serious obstacle in interactions leading to new-frequency generation, i.e. when $\omega_4 \neq \omega_1, \omega_2$, and ω_3 . (e.g. section VI on THG). When the nonlinear polarization is at one of the driving frequencies, $\omega_4 = \omega_i$ for example, conservation of energy (Eq.4) implies that $\omega_j = -\omega_k$. In this case, Eq.(5) reduces to a “vector matching” condition that depends only on the geometry (i.e. direction) of the beams (Sections XI and XII).

The frequency terms arising from the third-order nonlinear polarization described by Eq. (1) are collected in Table I. In the following section, we discuss the physical mechanisms and important features of these processes.

II. Quantum Mechanical Picture

The conservation of energy shown in the frequency summation of Eq. (4) contains both positive and negative signs from each of the input beams. A positive sign represents the annihilation (absorption) of a photon while the negative sign is interpreted as the generation (gain) of a photon. Both annihilation and generation of photons involve atomic and/or molecular transitions from one state to another. It is instructive to use diagrams to keep track of transitions participating in the nonlinear interactions. Let us take the most general case where four distinguishable beams (i.e. three input photons at $\omega_1, \omega_2, \omega_3$ and the final photon at ω_4) are involved. The third-order nonlinear interaction follows a path corresponding to one of 14 sign ordering possibilities, assuming emission at the photon frequency ω_4 . All possible time-ordering sequences are illustrated in Fig.1. In addition, the interacting photons are in general distinguishable; we have not shown this in Fig. 1 to preserve the clarity of presentation. Because the photons are (in general) distinct, we must allow for permutation of frequencies in the diagrams. Assuming emission at ω_4 (i.e. we can only assign ω_4 to a downward pointing arrow), we count up the various time ordering permutations for each interaction path shown in Fig. 1. This gives a total of 168 terms! Little would be gained by a tedious analysis of all these terms and such a task is far beyond the scope of this chapter. Instead, we illustrate some important third-order mechanisms and the role of resonances in Fig. 2, where we have labeled the three most important diagrams in Fig. 1. The energy level $|g\rangle$ is the ground state while $|a\rangle, |u\rangle$, and $|b\rangle$ are intermediate states of the system in a sequence of transitions involving photons with frequencies $\omega_i, \omega_j, \omega_k$, and ω_l ($i,j,k,l = 1,2,3,4$) such that $\pm\omega_i \pm \omega_j \pm \omega_k \pm \omega_l = 0$. The three time-ordering processes shown in the figure are:

Fig.2(a) Consecutive absorption of three photons followed by the generation of the final photon, partly describing sum frequency generation and third-harmonic generation. The reverse process is third-order parametric amplification, which is the absorption of a photon together with emission of three photons.

Fig.2(b) An absorption-emission-absorption-emission sequence. Difference frequency generation and frequency mixing are examples of this type of interaction. Coherent anti-Stokes Raman spectroscopy (CARS) is also represented by this transition sequence.

Fig.2(c) Absorption of two photons followed by emission of the two photons. As can be seen in the third section of in Table 1, a variety of physical mechanisms fall under this general description. Note the essential difference between (b) and (c) is the time ordering of the transitions. This is extremely important in resonant cases: a Raman-type resonance occurs in (b), and a two-photon resonance exists in (c).

Energy conservation is strictly obeyed upon the completion of the interaction (as dictated by Eq.(4)) but may be violated in the time frame of intermediate state transitions. This is allowed by Heisenberg's Uncertainty Principle. In many cases, an intermediate state is a "virtual" state, which is a convenient way of stating that a real, intermediate state of the system does not exist to support the transition of a photon at the selected wavelength. The virtual, intermediate state allows for energy bookkeeping in transition diagrams, but a physical description of the optical interaction using quantum mechanics involves only real eigenstates of the system. In particular, there must be a dipole-allowed transition between the initial state $|g\rangle$ and a real state "associated" with the virtual state. The timescale and strength of the interaction is partly determined by the energy mismatch between the virtual, intermediate state and an associated real, electronic state. This means a system can absorb a photon of energy $\hbar\omega_i$ and make a transition from the ground state $|g\rangle$ to a real intermediate state $|a\rangle$ even though there is insufficient photon energy to bridge the gap, i.e. there is an energy mismatch $\Delta E = |\hbar\omega_i - E_a + E_g| > 0$. This is possible provided the interaction occurs in a time faster than the observation time $\Delta t \sim \hbar/\Delta E$ permitted by the Uncertainty Principle. Transitions of this type are called virtual transitions as opposed to real transitions where energy is conserved. In the former case, Δt is known as the virtual lifetime of the transition.

If the entire sequence of transitions comprising the third-order interaction is not completed within the virtual lifetime, the intermediate state collapses back to the ground state and no nonlinear interaction occurs. In other words, all the required particles must be present in the system during the virtual lifetime. The longer the virtual lifetime, the greater the probability that the required photons will appear allowing the multi-particle interaction to run to completion. A longer virtual lifetime translates to a larger third-order nonlinear susceptibility $\chi^{(3)}$. The closer an input photon moves to a dipole-allowed system resonance, the longer the virtual lifetime and the resulting $\chi^{(3)}$ gets stronger.

These quantum mechanical issues are manifest in the mathematical formulation of $\chi^{(3)}$ derived from perturbation theory [1, 3, 17]

$$\chi^{(3)}(\pm\omega_1, \pm\omega_2, \pm\omega_3) = \frac{N}{\hbar^3} \sum_{i,j,k,l} \sum_{a,u,b} \mu_{ga} \frac{\mu_{au}}{(\omega_{ag} \mp \omega_i)} \frac{\mu_{ub}}{(\omega_{ug} \mp \omega_i \mp \omega_j)} \frac{\mu_{bg}}{(\omega_{bg} \mp \omega_i \mp \omega_j \mp \omega_k)} \quad (6)$$

In Eq. (6), N is the total population in the ground state $|g\rangle$ and μ 's are dipole-moment matrix elements associated with each of the transitions. The first sum describes the frequency permutations: i,j,k and l can take any integer value 1,2,3,4, provided energy conservation ($\pm\omega_i \pm \omega_j \pm \omega_k \pm \omega_l = 0$) is obeyed. The second sum is over all possible real, intermediate quantum eigenstates of the system. This complicated looking equation is nothing more than the sequence of optical transitions weighted by the appropriate virtual lifetime. The first coefficient represents the virtual transition initiated by a photon of energy $\hbar\omega_i$ from the ground state to the intermediate

state $|a\rangle$ with strength given by the matrix element μ_{ga} . The next three matrix elements are weighted by the virtual lifetimes of their initial state. The virtual lifetimes are represented by energy (i.e. frequency) denominators; as the photon frequency approaches a system resonance, the virtual lifetime and magnitude of $\chi^{(3)}$ grow accordingly.

The \pm signs in front of the frequency arguments in Eq. (6) indicate there is a physical significance to the time ordering of the participating photons. This representation distinguishes the various components of the third-order susceptibility. In many textbooks, a permutation of all the frequencies (including the signs) is already incorporated in the final calculation of $\chi^{(3)}$ [3, 4]. In that case, for a given ω_4 , one obtains the total contribution to $\chi^{(3)}$ with the order of frequency arguments having no particular physical relevance.

We also point out that the nonlinear susceptibility described by the above equation and shown in our example is *real*. A resonance condition occurs when any one of the energy/frequency denominators approaches zero. This not only enhances $\chi^{(3)}$ but also makes it a complex quantity, i.e. a resonance condition introduces an imaginary component to $\chi^{(3)}$. This is better understood by making the following substitution:

$$\frac{1}{\Delta\omega} \rightarrow \frac{1}{\Delta\omega + i\Gamma} \quad (7)$$

where Γ represents a phenomenological broadening of the particular transition. This complex damping term accounts for the physical impossibility of the nonlinear susceptibility becoming infinite in a resonance condition. Even in the case of vanishing damping, a basic theorem of complex variables can be applied to Eq. (7):

$$\lim_{\Gamma \rightarrow 0} \frac{1}{\Delta\omega + i\Gamma} = \wp\left(\frac{1}{\Delta\omega}\right) + i\pi\delta(\Delta\omega), \quad (8)$$

where \wp stands for the principle value and δ is the Dirac delta function. The important message is that in general, the nonlinear susceptibility $\chi^{(3)}$ is a complex quantity that will be dominated by its imaginary component when photon frequencies move into resonance with real eigenstates of the system. The resonance conditions leading to a strong imaginary $\chi^{(3)}$ are associated with one or more of the following processes: three-photon ($\omega_i + \omega_j + \omega_k = -\omega_l \approx \omega_{bg}$), two-photon ($\omega_i + \omega_j = -\omega_k - \omega_l \approx \omega_{bg}$), Raman-type ($\omega_i - \omega_j = \omega_l - \omega_k \approx \omega_{ig}$), and/or single-photon ($\omega_i \approx \omega_{ag}$) resonances. The latter cases (i.e. those having linear resonance) will be discussed in Section IX, which deals with cascaded $\chi^{(1)}:\chi^{(1)}$ nonlinearities. A special case of linear resonance can occur in Raman-type transitions where $\omega_{ig}=0$, i.e. when the second intermediate state is degenerate with the ground state. This corresponds to the optical Stark effect (ac Stark effect). The three-photon resonance that gives rise to an imaginary $\chi^{(3)}$ in third-harmonic generation does not have a significant physical implication. It only influences the phase of the interacting fields, similar to the case of second-order effects (e.g. second-harmonic generation) [1]. The remaining two processes involving two-photon and Raman resonances are of significant interest and will be discussed in detail.

III. Nonlinear Absorption (NLA) and Nonlinear Refraction (NLR)

Just as the real and imaginary components of the linear susceptibility $\chi^{(1)}$ are associated with refraction and absorption, the real and imaginary parts of $\chi^{(3)}$ describe nonlinear refraction (NLR) and nonlinear absorption (NLA) or gain. This can be understood by considering situations in

which the nonlinear polarization is at one of the driving frequencies. These are particular cases of Figs. 2(b) and 2(c), with corresponding polarization terms given in the third row of Table 1. Taking the interacting photons to have frequencies ω_a and ω_b , the total polarization (linear and third order) at ω_a can be written as:

$$P(\omega_a) = \varepsilon_0 \left\{ \frac{1}{2} \chi^{(1)}(\omega_a) E_a + \frac{3}{8} \chi^{(3)}(\omega_a, \omega_a, -\omega_a) E_a^2 E_a^* + \frac{6}{8} \chi^{(3)}(\omega_a, \omega_b, -\omega_b) E_a E_b E_b^* \right\}. \quad (9)$$

For the sake of brevity, we ignore time-ordering in the frequency arguments of $\chi^{(3)}$. This means that the $\chi^{(3)}$ component in the above equation is assumed to contain the various permutations of frequencies including, for example, two-photon as well as Raman transitions shown in Figs. 2(b) and 2(c). From Eq. (9), we introduce an effective susceptibility χ_{eff} :

$$\chi_{\text{eff}}(\omega_a) = \chi^{(1)}(\omega_a) + \frac{3}{4} \chi^{(3)}(\omega_a, \omega_a, -\omega_a) |E_a|^2 + \frac{6}{4} \chi^{(3)}(\omega_a, \omega_b, -\omega_b) |E_b|^2. \quad (10)$$

Deriving the coefficients of nonlinear absorption and refraction from Eq. (10) is now straightforward. The complex refractive index is defined as:

$$n + i\kappa = (1 + \chi_{\text{eff}})^{1/2}. \quad (11)$$

Making the very realistic assumption that the nonlinear terms in Eq. (10) are small compared to the linear terms, we use the binomial expansion to simplify Eq. (11):

$$n + i\kappa \cong n_0 + i \frac{c}{2\omega_a} \alpha_0 + \Delta n + i \frac{c}{2\omega_a} \Delta \alpha, \quad (12)$$

where $n_0 = (1 + \Re\{\chi^{(1)}\})^{1/2}$. We also assume the background linear absorption coefficient is small, i.e. $\alpha_0 \propto \Im\{\chi^{(1)}\} \ll \Re\{\chi^{(1)}\}$. We define the irradiance as $I_i = (1/2)c\varepsilon_0 n_0(\omega_i) |E_i|^2$ ($i=a,b$) and the nonlinear refraction coefficient n_2 and the nonlinear absorption coefficient α_2 as follows:

$$n_2(\omega_a; \omega_b) = \frac{3}{4\varepsilon_0 n_0(\omega_a) n_0(\omega_b) c} \Re\{\chi^{(3)}(\omega_a, -\omega_b, \omega_b)\}, \quad (13)$$

$$\alpha_2(\omega_a; \omega_b) = \frac{3\omega_a}{2\varepsilon_0 n_0(\omega_a) n_0(\omega_b) c^2} \Im\{\chi^{(3)}(\omega_a, -\omega_b, \omega_b)\}. \quad (14)$$

The change of refractive index due to the presence of fields E_a and E_b is:

$$\Delta n(\omega_a) = n_2(\omega_a; \omega_a) I_a + 2n_2(\omega_a; \omega_b) I_b, \quad (15)$$

and the change of absorption is

$$\Delta \alpha(\omega_a) = \alpha_2(\omega_a; \omega_a) I_a + 2\alpha_2(\omega_a; \omega_b) I_b, \quad (16)$$

where I_a and I_b are the irradiances of the two beams. Note that, without loss of generality, we assume the measurement is performed on the laser beam corresponding to field E_a while the field E_b acts as an excitation source only. The first terms on the right-hand-side of the above equations correspond to self-action (i.e. commonly performed single beam experiments). The second terms correspond to the case of an excite-probe experiment where the two beams are distinguishable either by frequency and/or wavevector. The factor of 2 in front of the second terms in Eq. (15) and (16) arises from the larger number of permutations in this component of the nonlinear susceptibility [3, 4, 31]. The stronger nondegenerate response (i.e. distinguishable beams) is sometimes referred to as weak-wave retardation [32]. While most reported measurements and applications involve degenerate self-action processes (i.e. a single laser beam), the theoretical treatment presented in this chapter considers the more general nondegenerate case. One must keep in mind that degenerate third-order coefficients are only the limit of the nondegenerate case where

$\omega_a = \omega_b$. The need for generality in the theoretical approach is very important for correct implementation of the Kramers-Kronig dispersion relations in nonlinear optics. This allows us to establish a rigorous mathematical relation between NLR and NLA, discussed in the next section.

Another commonly used coefficient for describing the nonlinear index is \tilde{n}_2 defined as:

$$n = n_0 + \tilde{n}_2(\omega_a; \omega_a) \frac{|E_a|^2}{2} + 2\tilde{n}_2(\omega_a; \omega_b) \frac{|E_b|^2}{2}. \quad (17)$$

where \tilde{n}_2 is usually given in Gaussian units (esu). \tilde{n}_2 is related to n_2 by

$$\tilde{n}_2(esu) = \frac{cn}{40\pi} n_2(SI), \quad (18)$$

where the right hand side is in SI/MKS units. The reader is cautioned that in the literature various symbols and definitions different from those given here are often used to describe the nonlinear refractive index. The symbol β is commonly used in place of α_2 to denote two-photon absorption (2PA).

The propagation of electromagnetic waves E_a and E_b through a nonlinear medium, ignoring the effect of diffraction and dispersion (i.e. pulse distortion) is governed by the following equations for the irradiance and phase of the probe beam (E_a):

$$\frac{dI_a}{dz} = -\alpha_0(\omega_a)I_a - \alpha_2(\omega_a; \omega_a)I_a^2 - 2\alpha_2(\omega_a; \omega_b)I_aI_b \quad (19)$$

and

$$\frac{d\phi_a}{dz} = \frac{\omega_a}{c} \left[n_0(\omega_a) + n_2(\omega_a; \omega_a)I_a + 2n_2(\omega_a; \omega_b)I_b \right] \quad (20)$$

The coefficient n_2 is often used to describe the nonlinear index change due to mechanisms such as thermally induced material changes, molecular orientation effects, saturation of absorption, and ultrafast $\chi^{(3)}$ processes. Here, consistent with our definition of $\chi^{(3)}$, we designate the n_2 notation for local and linearly nonresonant nonlinearities only. Processes that appear as an ‘‘effective’’ n_2 are treated separately as cascaded $\chi^{(1)}:\chi^{(1)}$ or $\chi^{(2)}:\chi^{(2)}$ phenomena.

As a consequence of the principle of causality, the real and imaginary parts of the linear susceptibility are connected through the Kramers-Kronig relations of linear optics. Eqs. (19) and (20) suggest a similar relation in nonlinear optics. We discuss the Kramers-Kronig relations of nonlinear optics and their underlying physics next.

IV. Kramers-Kronig Dispersion Relations

The complex response function of any linear, causal system obeys a dispersion relation linking its real and imaginary parts as Hilbert transform pairs. In linear optics, causality is manifest in the Kramers-Kronig (K-K) dispersion relations (Chapter 36) that tie the frequency dependent refractive index, $n(\omega)$, to the absorption coefficient $\alpha(\omega)$ and vice-versa.:

$$n(\omega) - 1 = \frac{c}{\pi} \wp \int_0^\infty \frac{\alpha(\omega')}{\omega'^2 - \omega^2} d\omega' \quad (21)$$

where \wp denotes the Cauchy principal value. The principal value is really just a warning to be careful when integrating near the singularity in the denominator of the integrand. We drop the \wp notation for simplicity although it is always implied. There is an equivalent relation for the real and imaginary parts of the linear susceptibility:

$$\Re\{\chi^{(1)}(\omega)\} = \frac{1}{\pi} \int_{-\infty}^{\infty} \frac{\Im\{\chi^{(1)}(\omega')\}}{\omega' - \omega} d\omega' \quad (22)$$

The K-K relation is the mathematical expression of causality and a simple, intuitive derivation of these relations can be made [33, 34].

Causality clearly holds for any real, linear system. Real, nonlinear systems must also be causal – does that imply there are dispersion relations as well? If so, what form do they take? The Kramers-Kronig relations of linear optics are derived from linear dispersion theory, suggesting this procedure is completely inappropriate for a nonlinear system. Fortunately, this is not the case and since the early days of nonlinear optics, many authors have addressed the K-K relations in the nonlinear regime. [35-38]. The usefulness of these relations was not fully appreciated until recently, however [31, 39, 40]. The key insight is that one can linearize the system; we view it as the material *plus* a strong perturbing light beam. This new linear system, which is different from the system in the presence of weak light, has a modified absorption spectrum. The linear Kramers-Kronig relation is applied in the presence of and in the absence of a high field perturbation and we study the difference between these two regimes. It is important to appreciate the fact that our new system is causal even in the presence of an external perturbation. This allows us to write down a modified form of the Kramers-Kronig relation linking the index of refraction to the absorption[31, 39]:

$$[n(\omega) + \Delta n(\omega; \zeta)] - 1 = \frac{c}{\pi} \int_{-\infty}^{\infty} \frac{\alpha(\omega') + \Delta\alpha(\omega'; \zeta)}{\omega'^2 - \omega^2} d\omega' \quad (22)$$

After subtracting the linear terms n and α , we are left with a relationship between the changes in refractive index and change of absorption:

$$\Delta n(\omega; \zeta) = \frac{c}{\pi} \int_0^{\infty} \frac{\Delta\alpha(\omega'; \zeta)}{\omega'^2 - \omega^2} d\omega' \quad (23)$$

where ζ denotes the perturbation. An equivalent relation also exists that allows calculation of the change in absorption coefficient given the change in the refractive index. This relation is rarely used in practice for reasons described momentarily. In evaluating Eq. (23), it is essential that the perturbation be independent of the frequency of observation (ω'). In other words, the excitation ζ must remain constant as ω' is varied.

It is an interesting fact that calculation of the refractive index change from data obtained in nonlinear optics experiments is often easier than extracting the absolute refractive index from the K-K transform in linear optics! The reason is that absorption changes in nonlinear optics are usually strong only in a very limited frequency range; the integration range in Eq. (23) need only consider this spectrum. In contrast, evaluation of the linear index based on the linear absorption spectrum normally involves a much larger amount of data. One must take full account of the entire linear absorption data to obtain quantitative agreement with experiments that measure the refractive index. In the same way, the reverse transformation in nonlinear optics (obtaining $\Delta\alpha$ from Δn) is not as accommodating as the transformation of Eq.(23). Experiments show that irradiance-dependent changes of the refractive index occur over a relatively broad frequency spectrum. A large and impractical amount of nonlinear dispersion data must be collected and incorporated into a K-K calculation of nonlinear absorption. The reverse transformation is thus difficult to accomplish in practice.

Eq. (23) has been used to determine refractive changes due to “real” excitations (i.e. $\chi^{(1)}$: $\chi^{(1)}$ cascaded processes) such as thermal and free-carrier nonlinearities in semiconductors[41] [42]. In these examples, ζ denotes either change of temperature or change of free-carrier density, respectively. This K-K methodology has also been applied with great success to the situation where the perturbation is “virtual” or non-resonant. This work unified the bound-electronic Kerr effect in bulk semiconductors (i.e. the dispersive nonlinearity resulting from anharmonic motion of bound, valence electrons) to its absorptive counterparts: two-photon absorption, the electronic Raman effect, and the ac Stark effect [31, 39, 43-45]. The dispersion relation between α_2 and n_2 is given by:

$$n_2(\omega_a; \omega_b) = \frac{c}{\pi} \int_0^{\infty} \frac{\alpha_2(\omega'; \omega_b)}{\omega'^2 - \omega_a^2} d\omega' . \quad (24)$$

Note that in the general case we are dealing with two frequencies, ω_a and ω_b . Even in the degenerate situation i.e. $n_2=n_2(\omega_a; \omega_a)$ where we desire the nonlinear index coefficient at a single frequency ω_a , we are still required to provide the nondegenerate absorption spectrum $\alpha_2(\omega'; \omega_b)$ at all frequencies ω' as input to the calculation. We also point out that Eq. (24) can be used to derive relations linking the real and imaginary parts of the nonlinear susceptibility via Eqs. (13) [the inverse transformation is obtained with Eq. (14)]:

$$\Re\{\chi^{(3)}(\omega_a, \omega_b, -\omega_b)\} = \frac{2}{\pi} \int_0^{\infty} \frac{\omega' \Im\{\chi^{(3)}(\omega', \omega_b, \omega_b)\}}{\omega'^2 - \omega_a^2} d\omega', \quad (25)$$

Using the symmetry properties of $\chi^{(3)}$, an equivalent representation is:

$$\Re\{\chi^{(3)}(\omega_a, \omega_b, -\omega_b)\} = \frac{1}{\pi} \int_{-\infty}^{\infty} \frac{\Im\{\chi^{(3)}(\omega', \omega_b, \omega_b)\}}{\omega' - \omega_b} d\omega'. \quad (26)$$

Eq. (26) can be also be derived in a very general way from a first-principles approach that applies the causality condition directly in the temporal nonlinear response. In this way, one can obtain the dispersion relations for the n-th order optical susceptibility [39]:

$$\chi^{(n)}(\omega_1, \omega_2, \dots, \omega_j, \dots, \omega_n) = \frac{-i}{\pi} \int_{-\infty}^{\infty} \frac{\chi^{(n)}(\omega_1, \omega_2, \dots, \omega', \dots, \omega_n)}{\omega_j - \omega'} d\omega', \quad (27)$$

where $\chi^{(n)}$ is a complex quantity. By separating the real and imaginary parts of this equation, we get the generalized Kramers-Kronig relation for a nondegenerate, n-th order nonlinear susceptibility:

$$\Re\{\chi^{(n)}(\omega_1, \omega_2, \dots, \omega_j, \dots, \omega_n)\} = \frac{1}{\pi} \int_{-\infty}^{\infty} \frac{\Im\{\chi^{(n)}(\omega_1, \omega_2, \dots, \omega', \dots, \omega_n)\}}{\omega' - \omega_j} d\omega'. \quad (28)$$

Note that for n=3 with the substitutions $\omega_1=\omega_a$, $\omega_2=\omega_b$ and $\omega_3=-\omega_b$, Eq. (28) becomes identical to Eq. (26). When the susceptibilities for generating frequency harmonics are included, Eq.(28) can be further generalized [39]. If we consider the $\chi^{(3)}$ associated with third-harmonic generation, it can be shown that:

$$\Re\{\chi^{(3)}(+\omega, +\omega, +\omega)\} = \frac{1}{\pi} \int_{-\infty}^{\infty} \frac{\Im\{\chi^{(3)}(+\omega', +\omega', +\omega')\}}{\omega' - \omega} d\omega'. \quad (29)$$

Such relationships have been utilized in calculations of the total $\chi^{(3)}$ (THG) in semiconductors. It is computationally more convenient to first calculate the imaginary part because of the presence of δ -functions in its frequency domain. The real part is then calculated using the K-K dispersion relations [46].

V. Optical Kerr Effect

The $\chi^{(3)}$ process leading to an intensity dependent refractive index is known as the Optical Kerr effect (OKE). Experimental observation is relatively straightforward, usually requiring just a single laser beam. The OKE is described by Eq. (15) where, for the sake of brevity, we ignore cross-modulation terms and drop the frequency terms to write:

$$n = n_0 + n_2 I \quad (30)$$

There are a variety of physical mechanisms that submit to this mathematical representation, many different ways to observe the effect experimentally, and an assortment of practical devices that can be built.

Optical transitions giving rise to a nonlinear susceptibility $\chi^{(3)}$ (see Figs. 1-2 for example) are intimately related to the energy eigenstates of the system. These eigenstates can be associated with bound electronic motion, molecular vibrations, or molecular rotations of the system. Electronic transitions involve the largest energy separation and rotational transitions the smallest. In a given material (gas, liquid, or solid), one or more of these excitations may contribute to the optical Kerr effect. In general, the various contributions differ in their response time, magnitude, and frequency dependence. Referring to our earlier discussion of Eq. (6), the time response of an optical nonlinearity is governed by the virtual lifetime of the relevant transitions. This implies that the nonlinearities associated with the electronic transitions give the fastest response time because they possess large energy denominators. Experiments have shown that electronic nonlinearities are usually faster than the time resolution provided by the shortest optical pulses available at the time of this writing (< 10 fs). For practical purposes then, the nonlinearity associated with the motion of bound electrons can be regarded as instantaneous. At the other extreme, the nonlinearity associated with rotational motion of molecules is relatively sluggish – response times in the picosecond regime have been measured. In the middle range are nonlinearities arising from molecular vibrations. For a Raman-type transition shown in Fig. 2-b, this effect is manifest as the Raman Induced Kerr Effect (RIKE). We discuss two important cases of NLR: the bound electronic Kerr effect in solids (n_2) and the rotational (or orientational) Kerr effect in liquids.

• *Bound Electronic Optical Kerr Effect in Solids*

The optical Kerr effect in solids has been extensively studied in materials ranging from large gap dielectrics and glasses to narrow gap semiconductors [31, 44, 47-50]. The fundamental energy gap E_g turns out to be a parameter of critical importance. Because of direct, linear absorption of the incident laser light, we are interested in the transparency regime where the photon frequency is less than the bandgap energy, i.e. $\omega < \omega_g = E_g/\hbar$. We estimate the response time (τ_r) of the nonlinearity using the virtual lifetime of the transition: $\tau_r \approx 1/|\omega - \omega_g|$. Far below the bandgap where $\omega \ll \omega_g$, the response time can be very fast ($\ll 10$ fs) and for most applications can be assumed as instantaneous. This ultrafast response has been exploited in soliton propagation in glass fibers [51] [5] (Section XI) and in the generation of femtosecond pulses in solid-state lasers (Kerr-lens mode-locking, Chapter 14) [52]. The optical Kerr effect also causes self-focusing, sometimes resulting in beam distortion and damage in transparent media (Section XI). Another significant application is the development of ultrafast all-optical-switching devices [53, 54]. Although much progress has been made in this area of research, development of a practical switch has been hindered by the relatively small magnitude of bound-electronic nonlinearities.

The bound-electronic optical Kerr effect in optical solids has been analyzed using semi-empirical methods [55] and, more recently, by simple two-band models appropriate for semiconductors [31, 44]. The latter treatment provides information about the dispersion, band-gap scaling, and the relationship between the NLA (e.g. two-photon absorption) and NLR through Kramer-Kronig transformation. The resulting simple formula allows one to predict the nonlinear refraction coefficient n_2 knowing only the photon frequency (ω), energy bandgap (E_g), and linear index (n_0):

$$n_2(m^2/W) = \frac{A}{n_0^2 E_g^4} \bar{G}_2 \left(\frac{\hbar\omega}{E_g} \right), \quad (31)$$

where $A \approx 3 \times 10^{-35}$ (MKS); E_g in Joules. The function \bar{G}_2 describes the normalized dispersion of the coefficient n_2 and is depicted in Fig. 3 along with the normalized two-photon absorption spectrum for bulk semiconductors (Section VIII).

Recall that NLA and NLR correspond to the imaginary and real parts of the third order susceptibility, respectively. The derivation of Eq. (31) by a Kramers-Kronig transformation required knowledge of the NLA spectrum. Three different mechanisms of NLA were employed in the analysis, corresponding to the three relevant time-ordering sequences depicted in Fig. 2: two-photon absorption, electronic Raman scattering, and the optical (a.c.) Stark shift of electronic states. The optical Stark effect is a change of the fundamental energy gap that occurs when the oscillating laser field becomes comparable to the electric field binding valence electrons to the positively charge nuclei. In experiments where only a single beam is used (i.e. all the input frequencies are the same), the only observable NLA effect is two-photon absorption, which is discussed in Section VIII.

The plot of the dispersion function \bar{G}_2 (Fig. 3) is consistent with our intuitive arguments about resonance enhancement presented in Sec. II. At long wavelengths (i.e. for $\hbar\omega \ll E_g$), we are far from resonance so $\bar{G}_2 \approx 1$ and is nearly frequency independent, i.e. there is very weak dispersion. Approaching the two-photon resonance, i.e. as $2\hbar\omega$ gets close to E_g , there is an approximately five-fold enhancement of n_2 . With increasing photon energy, the sign of n_2 reverses; this is a direct consequence of the sign change in the energy denominator associated with two-photon absorption. With further photon energy increase, there is enhancement due to resonances ascribed to two-photon absorption and the optical Stark effect. The inverse fourth power bandgap scaling (i.e. E_g^{-4}) and the dispersion predicted by this simple expression display remarkable agreement with data obtained with many different semiconductors and dielectrics [44].

- ***Re-Orientalional Kerr Effect in Liquids***

The re-orientational Kerr effect involves transitions between rotational energy levels of a molecule. It is non-resonant and therefore associated with the real part of $\chi^{(3)}$. The absorptive nonlinearity associated with these rotational levels gives an imaginary component to $\chi^{(3)}$; this is a Raman-type transition known as Rayleigh-wing scattering [3, 17]. For simplicity, we make a classical description of this phenomenon. Consider a carbon disulfide (CS_2) molecule as shown in Fig. 4. This is a cigar-shaped molecule with different polarizabilities along its principle axes (here we show $\alpha_3 > \alpha_1$). As discussed in Section VII, the polarizability describes the propensity for an external field to produce a dipole in a molecule. In the first step of the interaction, the optical

field polarizes this molecule (i.e. induces a dipole moment). The induced dipole interacts with the applied field and aligns itself along the direction of polarization. This molecular re-orientation (rotation) causes a birefringence in an isotropic solution; initially, the molecules were randomly oriented and there was no birefringence. The response time of the molecule depends on its mass: the heavier molecule, the slower the response. As an example, CS₂ has a re-orientational $n_2 \approx 3.4 \times 10^{-18} \text{ m}^2/\text{W}$ with a relaxation time $\tau \approx 1\text{-}2 \text{ ps}$ [56].

VI. Third-harmonic generation

In crystals where there is no inversion symmetry, $\chi^{(2)}$ vanishes making sum and difference frequency mixing impossible. The possibility of third harmonic generation always exists in principle, although it usually suffers from practical drawbacks. Typical values of $\chi^{(3)}$ are orders of magnitude smaller than $\chi^{(2)}$ coefficients found in popular frequency conversion crystals. This means the laser irradiance must be increased to compensate, often leading to material damage. Third-harmonic generation in crystals is usually difficult to phase match as well (Chapter 36). Because of these obstacles, cascading of two second-order effects (second-harmonic generation followed by sum-frequency generation) in two separate crystals is usually the preferred method of obtaining high multiples of the pump laser frequency (see Section X).

Gases do not have the damage limitations of crystals. Third-harmonic generation was extensively studied in many different gases around the time high power, Q-switched lasers became widely available and conversion efficiencies as high as several percent were obtained. Studies of sodium vapor have been helpful in elucidating the resonant enhancement that occurs near ω , 2ω , and 3ω .

VII. Stimulated Scattering

Useful spectroscopic information can be obtained when light is scattered from material, often at frequencies far removed from absorption and emission resonances. Spontaneous scattering is a linear process, in which the material is unmodified by the probing light beam. The various forms of spontaneous scattering: Raman, Brillouin, and Rayleigh have been known for the better part of a century. In the presence of a sufficiently intense laser beam, however, these scattering processes can be strongly amplified by a nonlinear interaction of the excitation beam with the material, resulting in stimulated scattering.

Raman scattering is most commonly described as the interaction of light with vibrational waves in a material (electronic and magnetic excitations can also be measured in Raman experiments). These vibrational frequencies are typically in the infrared, meaning that Raman scattered light can have a substantial spectral shift with respect to near-infrared or visible excitation light. Brillouin scattering involves the interaction of light with acoustic waves – waves associated with the propagation of pressure in the medium leading to periodic density fluctuations. Acoustic waves occur at frequencies that are orders of magnitude smaller than material vibrations; Brillouin scattered light is therefore frequency shifted from the incident light by a much smaller amount. Rayleigh scattering results from the interaction of light with stationary density variations – variations much smaller than the wavelength of the incident light. Scattering takes place without any frequency shift relative to the incident light. Rayleigh scattering is of interest because of its strong wavelength dependence and polarization properties. Spontaneous scattering processes scale linearly with input irradiance.

- ***Stimulated Raman Scattering***

In Raman scattering (Fig. 5), a photon is absorbed by a material that makes a quantum-mechanical transition from a low energy state $|1\rangle$ to a high energy state $|2\rangle$. At some short time later (i.e. not instantaneously), the material relaxes to a lower energy state $|3\rangle$ different from the original state, giving up its energy in the form of a photon of different energy than the excitation photon. If the lower state $|3\rangle$ is at a higher energy than state $|1\rangle$, the emitted photon will be at a longer wavelength than the excitation light. This is called Stokes shifted Raman scattering. If the terminal state $|3\rangle$ is at a lower energy than state $|1\rangle$, the emitted photon will be shorter in wavelength than the incident light, leading to anti-Stokes shifted Raman scattering. The difference between the incident and emitted light thus provides information about the relative positions of the different energy levels. Maintaining the same nomenclature, there is also Stokes and anti-Stokes shifted Brillouin scattering. Note that when state $|1\rangle$ and $|3\rangle$ are the same, there is no frequency shift and we have Rayleigh scattering.

The intermediate state can be a real state corresponding to a quantum mechanical energy level of the system; this is known as resonant Raman scattering. In the theme of this chapter, resonant Raman scattering is an example of a cascaded linear process leading to an effective $\chi^{(3)}$. More often, the intermediate level is not resonant with the photon and the transition from $|1\rangle$ to $|2\rangle$ is virtual (illustrated by a horizontal dotted line in Fig. 5). The distinction between the resonant and non-resonant processes can be confusing because both are referred to as Raman scattering. To maintain consistency with standard nomenclature, we briefly depart from the logical organization of this chapter and discuss both resonant and non-resonant Raman scattering in this section

The essential physics of Raman scattering can be understood from the classical picture of a diatomic molecule of identical atoms vibrating back and forth at frequency ω_L . The diatomic molecule is an illustrative example; in principle all Raman-active and some normal modes of vibration of a solid, liquid, or gas can be probed with Raman techniques [57]. We assume that the electronic charge distribution on the molecule is perfectly symmetric, hence there is no permanent dipole or a dipole moment modulated by the vibration. This normal mode is therefore not dipole active, i.e. it cannot absorb electromagnetic radiation (see Chapter 9).

When an external electric field is applied, the situation changes. The field in an electromagnetic wave polarizes the charge distribution on the molecule and it acquires a dipole. If the induced dipole is also modulated by a normal mode of vibration, the mode is said to be Raman active. The extent to which an external field can polarize the molecule is quantified by the following equation:

$$\mathbf{p}(r,t) = \alpha \mathbf{E}(r,t) \quad (32)$$

where $\mathbf{p}(r,t)$ is the induced dipole moment, α is the polarizability, $\mathbf{E}(r,t)$ is the time- and spatially-varying electric field, and bold type denotes vector quantities. The polarizability is not constant, however, but a function of the molecular separation distance q . Writing the first two terms of a Taylor series expansion of $\alpha(q)$ we have:

$$\alpha(q) = \alpha_o + \left(\frac{\partial \alpha}{\partial q} \right)_{q_o} q \quad (33)$$

where α_o is a constant representing the polarizability at the equilibrium position of the molecule (q_o). The molecule vibrates at a frequency $\pm\omega_L$, which is the energy difference between the states $|1\rangle$ and $|3\rangle$ in Fig. 5, hence:

$$q = q_o \exp(\pm i\omega_L t). \quad (34)$$

Inserting Eqs. (33) and (34) into (32), and realizing that the electromagnetic field varies sinusoidally at the optical frequency ω , we find that the second term in the polarizability expansion is responsible for the appearance of induced dipoles oscillating at a frequency offset from the incident electromagnetic wave by $\pm\omega_L$:

$$\mathbf{p}(r,t)_{\text{Raman}} = \mathbf{E}_o(r) \left(\frac{\partial \alpha}{\partial q} \right)_{q_o} q_o \exp(i\omega t \pm i\omega_L t). \quad (35)$$

These dipoles can radiate and are the origin of spontaneous Raman scattering. There is also an oscillating dipole unaffected by the vibration corresponding to the term α_o . This dipole oscillation is exactly at the frequency of the incident light and corresponds to spontaneous Rayleigh scattering:

$$\mathbf{p}(r,t)_{\text{Rayleigh}} = \mathbf{E}_o(r) \alpha_o \exp(i\omega t). \quad (36)$$

In stimulated scattering, we have to consider the force exerted on the vibrating molecule by the external field as a consequence of its polarizability. This force involves only the second term in Eq. (33):

$$F = \frac{1}{2} \left(\frac{\partial \alpha}{\partial q} \right)_{q_o} \langle E^2(r,t) \rangle \quad (37)$$

where the angular brackets represent a time average over an optical period. In a dipole-active interaction, the lowest order forcing term is proportional to E resulting in linear absorption of light. In the case of a Raman-active mode, Eq. (37) shows the force scales as E^2 ; therefore the force is nonlinear in the field. The forcing term is negligible at low light intensities, but becomes important when large electromagnetic field levels generated by lasers are encountered.

Because the Raman active mode of the molecule is subject to a force proportional to E^2 , there must be two input photons driving the interaction. If the two photons are at different frequencies, the molecule will experience a force at the beat frequency of the two photons. If the wavelengths of the two photons are chosen so that their beat frequency equals that of the molecular vibration ω_L , strong amplification of all three waves (two input electromagnetic waves and the molecular vibration) can occur resulting in stimulated scattering. The molecular polarizability thus acts as a nonlinear mixing term to reinforce and amplify the interacting waves. It is important to realize this is of practical consequence only when the input electromagnetic fields are sufficiently high.

The nonlinear polarizability impresses sidebands on the pump light resulting in three distinct electromagnetic waves (laser beam, Stokes shifted Raman, and anti-Stokes shifted Raman) propagating in the medium. The same nonlinear mixing process that led to the generation of the Raman sidebands in the first place can cause coherent excitation of additional molecules due to their polarizability. In this way, a coherent vibrational wave builds up, which in turn feeds more energy into the Raman shifted components, thus amplifying them. In stimulated scattering, the fluctuations of the optical medium (vibrations, density variations, etc) are *induced* and *amplified* by the external electromagnetic radiation. In contrast, spontaneous scattering originates from the naturally occurring (thermally driven, for example) fluctuations of the material. Because the linear optical properties of the medium are modified by the presence of an exciting laser beam (specifically its irradiance), the various stimulated scattering mechanisms are classified as third-order nonlinear optical processes.

In stimulated Raman scattering (SRS), one is most often looking for a new frequency generation at the wavelength corresponding to the energy difference of levels $|2' \rangle$ (or $|2 \rangle$) and $|3 \rangle$ shown in Fig. 5. Stimulated Raman gain and loss applied to an input beam at this frequency can be obtained as well. Polarization effects occurring in the nonlinear wave mixing process can also be studied in what is known as Raman-induced Kerr effect spectroscopy (RIKES, see Chapter 36). We also mention two other classes of third-order nonlinear spectroscopy: coherent anti-Stokes Raman spectroscopy (CARS) and coherent Stokes Raman spectroscopy (CSRS). In these interactions, illustrated in Fig. 6, two external laser fields at frequencies ω_1 and ω_2 are supplied. There must be a third-order nonlinear polarization present as in SRS, leading to frequency mixing and new wavelengths.

The somewhat subtle differences distinguishing SRS, CARS, and CSRS are the number and location of intermediate levels (designated by dashed lines in Fig. 6). Consider two excitation frequencies with $\omega_1 > \omega_2$ probing a given material system with real energy levels separated by frequency ω_L in Fig. 6. In CARS, short wavelength photons are detected at $\omega_{as} = 2\omega_1 - \omega_2$. For the CSRS arrangement, the excited intermediate states are at lower energy and a longer wavelength photon at frequency $\omega_s = 2\omega_2 - \omega_1$ is detected. Note that SRS is obtained when the intermediate levels are degenerate; SRS is thus a special case of the nonlinear interaction. In linear, spontaneous Raman scattering, a single exciting electromagnetic wave is required. In SRS, two input fields are involved; they just happen to be at the same frequency and are invariably supplied by a single laser source. Unlike spontaneous Raman scattering, however, SRS is a function of the third-order nonlinear susceptibility and hence depends nonlinearly on the irradiance of the excitation laser.

It is important to emphasize that all three of these stimulated Raman processes (SRS, CARS, CSRS) are essentially a mixing of three waves to produce a fourth wave via the third-order nonlinear polarization. Analysis of the problem is made using second-order perturbation theory in quantum mechanics. The tensor nature of the third-order susceptibility and the multitude of ways the interacting waves of various polarization states can mix lead to complicated expressions. One finds resonance denominators quantifying the efficiency of the wave mixing process. The scattering efficiency is governed by the proximity of photon energies to real energy eigenstates in the system. In principle, SRS, CSRS, and CARS can all take place in an experiment; the various generated beams can be distinguished by substantially different angles of propagation when leaving the irradiated sample. These angles are readily determined by phase-matching conditions for the nonlinear interaction. The wave-vectors of the interacting photons can be arranged for maximum output signal of the desired Raman process. The phase matching condition is obtained automatically in SRS, but careful orientation of the interacting beams can lead to very narrow linewidths and extremely accurate spectroscopic measurements. Some applications of stimulated Raman scattering include high resolution spectroscopy of gases [11, 17, 58, 59], spin-flip Raman scattering, stimulated polariton (the quanta of photon-phonon coupling) scattering, and ultrafast time-resolved measurements [60, 61]. The reader should also be aware that Raman spectroscopy beyond the third-order nonlinear susceptibility has been demonstrated. Further information can be obtained in texts on nonlinear laser spectroscopy [3, 6, 10, 16, 62-65].

- ***Stimulated Brillouin Scattering***

Stimulated Brillouin scattering (SBS) is an important third-order nonlinear optical effect that has been widely used for efficient phase conjugate reflection of high power lasers [26]. An incident

laser beam can scatter with the periodic refractive index variations associated with a propagating acoustic wave. The scattered light, depending on the propagation direction of the acoustic wave, will be Stokes or anti-Stokes shifted by the frequency of the acoustic wave. The process is stimulated because the interference of the incident and scattered wave can lead to an amplification of the acoustic wave, which then tends to pump more energy into the scattered wave. This positive feedback process can cause an exponential growth of the SBS beam and very high efficiencies in the right circumstances. Optical feedback to the medium is accomplished in one of two ways: 1) *Electrostriction* is local compression of the material in response to the strength of the electromagnetic field with a commensurate refractive index change; 2) *Linear optical absorption* by the laser field leads to local heating, expansion, density fluctuations, and thus periodic modulation of the refractive index. The latter effect is an example of a cascaded $\chi^1:\chi^1$ process, which is the subject of Section IX. Electrostriction is usually associated with SBS and we discuss it here.

Consider again the diatomic molecule that was used to illustrate the Raman effect. In the presence of an external electric field, it acquires a polarizability described by Eq. (33). As we have seen, the induced dipole can interact with the field. Electrostriction accounts for the ability of the electric field to do work on the polarized molecule – pulling and pushing it by electrostatic forces. The molecules will move and tend to pile up in regions of high field, increasing the local density. Associated with these density changes will be a change of refractive index. Density fluctuations can also be generated by the change in pressure that accompanies a propagating acoustic wave: pressure nodes will exist in the peaks and valleys of the acoustic wave. Electrostriction therefore provides a coupling mechanism between acoustic waves and electromagnetic waves.

It is important to emphasize that the periodic modulations in an electrostrictive medium are propagating spatial fluctuations modulated at the frequency of traveling acoustic waves. When the density fluctuations are stationary, we can have stimulated Rayleigh scattering. A thorough, detailed discussion of the many (often intricate) issues in stimulated Brillouin and Rayleigh scattering can be found in textbooks on nonlinear optics [3, 11, 16, 17, 28].

VIII. Two photon Absorption

Two-photon absorption (2PA) is the process by which the energy gap between two real states is bridged by the simultaneous (in the context of the Uncertainty Principle discussed in Section II) absorption of two photons, not necessarily at the same frequency. Both photons have insufficient energy to complete the transition alone; 2PA is thus observed in the spectral range where the material is normally transparent. When the two photons are present *together* for a fleeting instant of time determined by the Uncertainty Principle, an optical transition can take place.

Quantum mechanically, we can think of the first photon making a virtual transition to a non-existent state between the upper and lower levels (Fig. 2-c). If the second photon appears within the virtual lifetime of that state, the absorption sequence to the upper state can be completed. If not, the virtual transition collapses back to the ground state and no absorption takes place. To have an appreciable rate of 2PA, photons must be supplied at a rate high enough that there is a reasonable probability two photons will both be present during the virtual lifetime. Because the

virtual lifetime is so short, photon fluxes must be high and therefore power levels from laser beams are required.

The efficiency of 2PA is affected by the proximity of the input photons to a real state of the system. It is important to note that there must be an allowed optical transition linking the initial state and this real state. The closer one of the input photons coincides with a real state, the stronger the 2PA. When the intermediate state of 2PA is also a system resonance, the situation is commonly referred to as excited state absorption (ESA) – a sequence of two linear absorption processes that leads to an effective third-order nonlinearity. Excited state absorption is thus a cascaded $\chi^{(1)}:\chi^{(1)}$ effect, giving rise to an effective third-order nonlinearity (Section IX). It has implications for optical power limiting and is discussed in Chapter [Optical limiting by Hagan] of this handbook.

In stimulated scattering, the *difference* frequency of two input electromagnetic fields $\hbar\omega_i - \hbar\omega_j$ equals a characteristic energy resonance of the material system. In 2PA, an energy resonance exists at the *sum* of the two input fields: $\hbar\omega_i + \hbar\omega_j$. In Secs. II and III, 2PA was shown to be associated with the imaginary part of $\chi^{(3)}$. This is because it is an absorption process, i.e. it is exactly resonant with two eigenstates of the system. It is the only NLA process (i.e. a process associated with the imaginary part of $\chi^{(3)}$) that can be simply studied with a single photon frequency.

Two-photon absorption in semiconductors is one of the most thoroughly studied subjects in the entire field of nonlinear optics [66]. The 2PA coefficient (often written β or α_2^{2PA}) of bulk semiconductors has been calculated using models involving only two parabolic bands and also with more complex band structure [67]. It is defined by the rate of electron-hole pair excitation: $dN/dt = \beta I^2/(2\hbar\omega)$. The two-parabolic band model gives a comparatively simple yet general and accurate description of 2PA for a large class of semiconductors. The theoretical result for single frequency excitation can be expressed as:

$$\beta(m/W) \approx \frac{B}{n_0^2 E_g^3} \bar{F}_2 \left(\frac{\hbar\omega}{E_g} \right) \quad (38)$$

where $\bar{F}_2(x) = 2(2x-1)^{3/2}/x^5$ and $B = 5.67 \times 10^{-66}$ ($x = \hbar\omega/E_g$ and the energy bandgap E_g is in Joules). The best empirical fit to experimental data is obtained with B adjusted to a slightly higher value of 9.06×10^{-66} . The function F_2 describes the dispersion of 2PA and is plotted in Fig. 3. The intimate relation between NLA and NLR and the role of 2PA in semiconductors is explored in Section IV and the following references [31, 67-69]. There are important practical implications for 2PA in semiconductors and dielectrics. It can enhance or degrade optical switching performance in semiconductor devices and lead to optical damage in laser window materials. 2PA is also the basis of Doppler-free spectroscopy of gases [57, 59].

IX. Effective third-order nonlinearities; cascaded $\chi^1:\chi^1$ processes

Effective third-order nonlinearities occur when one of the transitions in our four photon interaction picture is resonant, providing a path of linear absorption. Linear absorption is a mechanism to directly couple laser light into the system – with sufficiently intense laser light, the

linear optical properties of a material can be modified. An effective third-order nonlinearity occurs when linear absorption affects the refractive index. We give some examples here.

- ***Optically generated plasmas***

Optical generation of stable plasmas is readily obtained in semiconductors and most studies of this subject have been made with these materials (Chapters 9, 36). For cascaded linear processes that we discuss here, the formation of a free electron-hole pair occurs by direct bandgap excitation by an incident photon. The optically produced carriers augment the background electron-hole density and the plasma remains electrostatically neutral. If the generation of an excess amount of plasma exceeds the rate of loss (by recombination or diffusion) on the timescale of interest, the plasma will modify the linear optical properties of the semiconducting material. The simplest way to see this is via the classical Drude model, where the refractive index of a metal or semiconductor is [70] [71]:

$$n = n_0 \sqrt{1 - \frac{\omega_p^2}{\omega^2}} \quad (39)$$

In this equation, ω is the angular frequency of the light, n_0 is the linear index in the absence of significant free carrier density, and ω_p is the density-dependent plasma frequency:

$$\omega_p = \sqrt{\frac{Ne^2}{m\epsilon}} \quad (40)$$

where N is the electron-hole pair density, e is the electronic charge, m is the reduced mass of the positive and negative charge carriers (electrons, holes, or ions), and ϵ is an appropriate background dielectric constant. Note that as the carrier density increases, the refractive index decreases. The material is usually excited by a laser beam with a non-uniform spatial profile such as a Gaussian, giving rise to negative-lensing and self-defocusing, assuming $\omega < \omega_p$.

The situation becomes complicated at densities where many-body effects become important or when the Drude model ceases to be valid. We also note that optical generation of plasmas can also occur as the result of nonlinear mechanisms in the presence of high laser fields and we aren't, of course, restricted only to solid-state plasmas. Examples of nonlinear plasma production are multi-photon absorption, laser-induced impact ionization, and tunneling. Because plasma generation and the concomitant refractive index modification are caused by a nonlinear optical process, the order of the nonlinearity is higher than three. Although high order nonlinearities are a rich subset of the field, they are not dealt with in this chapter. A number of review articles and textbooks on laser-induced change to the refractive index due to plasma generation via linear absorption are available [31, 42, 72-74].

- ***Absorption Saturation***

Absorption saturation is a well-known example of a cascaded linear process. Consider a homogeneously broadened system of two-level atoms (i.e. a system of identical two-level atoms) with energy diagram shown in Fig. 7. The lower and upper states are resonant with a photon depicted by the vertical arrow and there is linear absorption of incident light. Associated with the absorption is a spectral linewidth (with a Lorentzian shape for a homogeneous system), illustrated on the right side of the diagram in Fig. 7. An induced dipole or polarization is set up between the two states upon excitation by a photon. The states are coherently coupled and this coherence is in phase with the exciting electromagnetic field. In a real system, this coherence will be quickly

destroyed by collisions with other atoms. The rate at which the coherence is “washed out” determines the spectral width of the absorption profile and hence the frequency response of the imaginary component of the linear susceptibility. The real part of the linear susceptibility is obtained by the Kramers-Kronig transformation, giving rise to what is traditionally known as anomalous dispersion of the refractive index shown on the left side of Fig. 7. Note that the refractive index is positive for frequencies below resonance and negative at frequencies above it.

We have assumed that the rate at which photons are supplied to the system produces a negligible change of population in the upper and lower states. This means that the rate of population relaxation (recombination and diffusion, for example) is much faster than excitation. When the incident irradiance is sufficiently high, however, this may no longer be the case. The upper level can become appreciably occupied, reducing the availability of terminal states for optical transitions. The absorption thus decreases or bleaches, indicated by the dashed lines in Fig. 7. Associated with the change of absorption is a change of refractive index. The relationship between absorption and refraction can again be handled with the Kramers-Kronig transformation *provided* we consider the system as being composed of both the atoms *and* the input light beam, specifically the nonequilibrium change of population created by the input light. This is exactly the same mathematical formulation used in the description of non-resonant third-order nonlinearities introduced in Section IV. The difference here is that the absorption of photons is a resonant, linear process. The linear absorption of light then affects the linear optical properties of absorption and dispersion. Because the reduction of absorption depends directly on laser irradiance, it behaves like a third-order nonlinearity. We point out that the resonant nature of absorption saturation (and the associated nonlinear refraction) can lead to an unacceptable deviation from a third-order susceptibility description when the input irradiance goes even higher. In the high power regime, a non-perturbative approach (i.e. not represented by a power series expansion) must be used [75].

Absorption saturation spectroscopy (with emphasis on gases) is discussed at length in Ref. [59]. It is also a principle nonlinear effect in bulk and quantum-confined semiconductors (where the simple two-level picture outlined above must be substantially modified), having implications for optical switching and bistability [42, 53, 72, 76]

We briefly mention the density matrix (see Volume II, Chapter 38, “Nonlinear Optics”). This is a powerful method of analysis for the resonant interaction of light with a two-level system. In addition to absorption saturation, the nonlinear optical effects described by the density matrix include Rabi oscillations, photon echoes, optical nutation, superradiance, self-induced transparency, and optical free induction decay, which are not immediately associated with a third-order nonlinearity derived from a perturbation expansion of the polarization. Experimental manifestations of the above phenomena, however, can often be represented by an effective third-order nonlinearity. The nonlinear optics of the two-level system and the associated optical Bloch equations derived from the density matrix formulation of the problem are discussed in the chapter of this volume entitled “Coherent Optical Transients”. The reader is also referred to many excellent textbooks and monographs [3, 11, 24, 77, 78].

- ***Thermal Effects***

Linear absorption of light must result in energy deposition in the irradiated material. If the rate of energy deposition significantly exceeds its rate of removal, heating can take place. As the energy of a collection of atoms and molecules increases, it's easy to understand that their macroscopic

optical properties will be altered. When there is a linear relationship between laser irradiance and the refractive index, an effective third-order nonlinearity will result. The thermo-optic effect has a relatively straightforward physical interpretation and is arguably one of the most important optical nonlinearities. It is often the power limiting mechanism of a high power solid-state laser – where excessive circulating optical flux can cause “thermal blooming” in the laser crystal. This heat-induced lensing effect can destroy the beam quality. Thermal-index coefficients have been extensively tabulated and the reader is referred to references [18] [42].

- **Photorefraction**

Photorefraction results from the spatial redistribution of electrons and/or holes in a solid (see Volume II, Chapter 39, “Photorefractive Materials and Devices”). Electron-hole pairs are generated by linear absorption of laser light. If the excitation geometry produces a spatial modulation of irradiance such as a two beam interference pattern, the electrons and holes will arrange themselves in accordance with the spatial irradiance profile. Often the linear absorption involves impurity levels. Mobile carriers tend to diffuse from the bright regions leaving fixed charges behind. If a sinusoidally modulated, two beam interference fringe pattern is written in a doped photorefractive crystal, for example, fixed charges of ionized states will be prevalent in the high irradiance regions while mobile charge carriers will tend to accumulate in regions with low light levels. A modulated space charge must exist and therefore a modulated electric field pattern must be present as well. This field alters the refractive index via the linear electro-optic effect (i.e. Pockel’s effect). The photorefractive nonlinearity is clearly non-local as it requires a spatial modulation of charge density. Manipulation of the carriers can also be obtained with static electric fields and the response time tends to be of the order of seconds [3] [79] [18, 80]

X. Effective third-order nonlinearities; cascaded $\chi^{(2)}:\chi^{(2)}$ processes.

Materials lacking a center of inversion symmetry have nonzero $\chi^{(2)}$ and exhibit a second-order nonlinear polarization. This is the second term in the polarization power series expansion of Eq. (1) that is responsible for the most well known effects in nonlinear optics including second-harmonic generation (SHG), sum and difference frequency generation (SFG), optical rectification (OR), and optical parametric processes [This volume, Chapter 38, “Optical Parametric Oscillators”]. It is also possible to cascade two $\chi^{(2)}$ processes to produce an effect that mimics a $\chi^{(3)}$ process. The most common and efficient way of producing THG, for example, is by a $\chi^{(2)}$ cascade process. In this interaction, an input source at ω generates SHG via the second order susceptibility $\chi^{(2)}$ ($2\omega=\omega+\omega$); the second harmonic and fundamental then mix in a second (or the same) nonlinear crystal to produce the third harmonic by sum frequency generation $\chi^{(2)}$ ($3\omega=2\omega+\omega$). This type of nonlinearity is nonlocal because the two processes (SHG and SFG) take place in spatially separate regions.

In addition to THG, all other $\chi^{(3)}$ effects have an analogous process in $\chi^{(2)}:\chi^{(2)}$ cascading. Consider the case where we have one frequency ω . The corresponding cascaded $\chi^{(2)}$ effects are depicted in Fig. 8. Recall that the intrinsic $\chi^{(3)}$ is manifest as: a) THG, b) 2PA, and c) the a.c. Stark effect. The horizontal block arrows indicate the point of cascade, i.e. the propagation of the beams between the two $\chi^{(2)}$ interactions. There are always two distinguishable $\chi^{(2)}$ interaction regions; hence $\chi^{(2)}:\chi^{(2)}$ is clearly non-local. We also point out that in general the photon frequencies can be different.

Although the analogy is limited, cascaded $\chi^{(2)}$ effects exhibit NLA and NLR mimicking $\chi^{(3)}$. In the case of SHG, for example, the manifestation of $\chi^{(3)}$ NLA is depletion of the pump beam. The utility of cascaded $\chi^{(2)}:\chi^{(2)}$ for producing large nonlinear phase shifts has been realized only recently [81-83]. The analysis of $\chi^{(2)}$ is relatively straightforward, involving the coupled amplitude equations governing the propagation of the interacting beams. For example, the nonlinear phase shift imposed on a fundamental beam (ω) as it propagates through an SHG crystal of length L with a phase mismatch $\Delta k = k(2\omega) - 2k(\omega)$ and assuming small depletion is [82]:

$$\Delta\phi \approx \tan^{-1}\left(\frac{\Delta k L \tan(\beta L)}{2 \beta L}\right) - \frac{\Delta k L}{2} \quad (41)$$

where $\beta = \sqrt{\left(\frac{\Delta k L}{2}\right)^2 + \Gamma^2}$, $\Gamma = \frac{\omega \chi^{(2)} |E_0|}{2c \sqrt{n(2\omega)n(\omega)}}$, and E_0 denotes the electric field of the fundamental beam. An effective $\chi^{(3)}$ can be obtained if we expand $\Delta\phi$ to lowest order in Γ and use $\Delta\phi = \omega L n_2^{\text{eff}} I/c$ to give [84]:

$$n_2^{\text{eff}} = \frac{8}{c^2 4\pi\epsilon_0} \frac{\omega d_{\text{eff}}^2 L}{n^2(\omega)n(2\omega)} \left[\frac{\pi}{\Delta k L} \left(1 - \frac{\sin(\Delta k L)}{\Delta k L} \right) \right] \quad (42)$$

Here $d_{\text{eff}} = \chi^{(2)}(2\omega = \omega + \omega)/2$ is the effective tensor component of the second-order nonlinear susceptibility for a given experimental geometry.

Phase mismatch is represented by the bracketed term in Eq.(42), plotted in Fig. 9. Also shown in Fig. 9 is the depletion of the fundamental beam which, on the same level of approximation, can be regarded as an ‘‘effective two-photon absorption’’ coefficient that scales as $\beta^{\text{eff}} \sim \text{sinc}^2(\Delta k L)$. Cascaded $\chi^{(2)}$ leads to an effective refractive index modulation (n_2^{eff}) and two-photon absorption (β^{eff}), but one should not conclude that the material’s index of refraction is altered or energy is deposited in the material. These coefficients describe only nonlinear phase shifts and the conversion of the fundamental beam to second-harmonic beams. The nonlinear phase shift from the $\chi^{(2)}:\chi^{(2)}$ process has been used to demonstrate nonlinear effects analogous to those observed previously with the intrinsic optical Kerr effect. These include self-focusing and self-defocusing [81], all-optical switching [85, 86], soliton propagation [87, 88] and laser-modelocking [89].

XI. Propagation Effects

When the nonlinear optical polarization $P^{\text{NL}}(t)$ is known, the propagation of optical fields in a nonlinear medium can be analyzed with the aid of Maxwell’s equations:

$$\nabla \times \nabla \times E + \frac{1}{c^2} \frac{\partial^2 E}{\partial t^2} = -\mu \frac{\partial^2 P}{\partial t^2}, \quad (43)$$

where $P(t)$ is the total polarization including the linear and nonlinear terms. The slowly varying envelope approximation (SVEA) is then usually made to reduce the above equation to a system of four coupled nonlinear differential equations for the four interacting fields. For ‘‘thin’’ nonlinear media where there is no significant distortion of the spatial beam and temporal shape upon propagation, the problem simplifies greatly. Equations (19) and (20) were obtained with this approximation. For ‘‘thick’’ nonlinear media, however, linear and nonlinear diffraction as well as dispersion cannot be ignored. In this section, we discuss two important propagation phenomena: self-focusing and soliton formation.

- **Self-focusing**

Self-focusing occurs in materials with a positive intensity dependent refractive index coefficient ($n_2 > 0$). Self-focusing (or Kerr-lensing) causes spatial collapse of the laser beam when it propagates through transparent optical materials, often leading to optical damage. It is a consequence of the non-uniform spatial profile of the laser beam [2, 3, 17, 18]. For a “thin” nonlinear material, one makes the so-called parabolic approximation for the nonlinear phase shift to obtain an approximate Kerr-lens focal length, assuming a Gaussian beam of radius w (1/e of the electric field profile) [90]:

$$f_{NL} \approx \frac{aw^2}{4Ln_2I}, \quad (44)$$

where L is the thickness of the medium, I is the irradiance, and $6 > a > 4$ is a correction term. Note that when n_2 is negative, Eq. (44) shows there will be a negative focal length and thus self de-focusing of the incident beam.

Eq. (44) is valid for $f_{NL} \gg L$ and $Z_0 \gg L$ where Z_0 is the diffraction length (Rayleigh range) of the incident beam. This is the so-called “external self-action” regime [91]. This approximation fails for thick nonlinear media and/or at high irradiance, i.e. “internal self-action”. Equation (43) must then be solved numerically. Analysis shows that self-lensing of a Gaussian beam overcomes diffraction at a distinct threshold power, i.e. the self-focusing threshold, given by the approximate formula [92] [90]:

$$P_{cr} \approx \frac{a\lambda^2}{8\pi n_2 n_0} \quad (45)$$

Note that for sufficiently thick media, the self-focusing threshold occurs at a critical power, not at a threshold irradiance, i.e. the power at which the self-focusing overcomes diffraction. Self-focusing and diffraction both scale with beam area thus canceling out the spot size dependence in Eq.(45). Self-focusing and self-defocusing (collectively called self-action effects) are often employed in optical limiting applications. Self-action is also the essential mechanism for mode locking cw solid-state lasers, commonly known as Kerr-lens mode-locking [93].

- **Solitons**

Soliton waves are realized in many different physical circumstances ranging from mechanical motion to light propagation. In general, they are robust disturbances that can propagate distortion-free for relatively long distances. The robustness of optical solitons can be manifest in the time domain (temporal solitons), transverse space (spatial solitons), or both (light bullets). Temporal solitons have been extensively studied in optical fibers because of their tremendous utility in long distance optical communication. They exist as a consequence of a balance between the competing effects of linear refractive index dispersion and nonlinear phase modulation.

Assume a single beam propagating in a long nonlinear waveguide characterized by an instantaneous nonlinear index coefficient n_2 and a linear refractive index $n(\omega)$. Ignoring spatial effects (i.e. diffraction), we write the electric field as $E(z, t) = A_0 u(z, t - z/v_g) \exp(i\omega_0 t - ik_0 z) + c.c.$. From Eq. (43), one derives a differential equation describing the evolution of the soliton field envelope $u(z, t)$ [3, 51, 94]:

$$-i \frac{\partial u}{\partial z} + \frac{k_2}{2} \frac{\partial^2 u}{\partial \tau^2} = \Delta k_{NL} |u|^2 u \quad (46)$$

Here $v_g = d\omega/dk|_{\omega=\omega_0}$ is the soliton pulse group velocity, τ is a retarded time $\tau = t - z/v_g$, $k_2 = d^2k/d\omega^2|_{\omega=\omega_0}$ gives the group velocity dispersion (GVD), and $\Delta k_{NL} = n_2 I_0 \omega_0 / c$ is the irradiance-dependent change of propagation wavevector. In MKS units, the peak intensity of the soliton pulse is $I_0 = n_0 \epsilon_0 c |A_0|^2 / 2$. Eq. (46) is called the nonlinear Schrödinger equation (NLSE) and can be solved exactly. One solution gives the fundamental soliton pulse:

$$u(z, \tau) = \text{sech}(\tau / \tau_0) e^{i\kappa z} \quad (47)$$

where $\tau_0^2 = -k_2 / \Delta k_{NL}$ is the soliton pulsewidth and $\kappa = -k_2 / 2\tau_0^2$. Note that the modulus of the soliton pulse envelope $|u|$ remains unperturbed upon propagation. For this solution to exist, the GVD (k_2) and the nonlinear refraction (Δk_{NL}) must have opposite signs. For transparent optical solids including silica glass optical fibers, the nonlinear index coefficient n_2 is almost always positive, which means that a negative GVD is required. In fused silica fibers, the point of balance is attained at a wavelength of $\lambda \approx 1.55 \mu\text{m}$. This is also a spectral region with very low absorption loss. This wavelength has become the standard for the telecommunications industry. Optical solitons in fibers were first reported by Mollenauer et al. [51].

Spatial solitons refer to the propagation of an optical beam without any change or distortion to its spatial irradiance distribution. In this type of soliton, a point of stability is achieved between linear diffraction (causing the beam to diverge) and nonlinear self-focusing. In the presence of a $\chi^{(3)}$ nonlinearity, a stable solution to the NLSE can be found in one spatial dimension only [95, 96]. Using a cascaded $\chi^{(2)}:\chi^{(2)}$ nonlinearity, however, two-dimensional spatial solitons (or solitary waves) have been demonstrated [87, 88]. Two-dimensional spatial solitons can be realized for a cascaded $\chi^{(2)}:\chi^{(2)}$ process because of its different behavior compared to $\chi^{(3)}$ at large nonlinear phase shifts. Specifically, cascaded $\chi^{(2)}:\chi^{(2)}$ exhibits a saturation of the nonlinear phase-shift that is a direct consequence of depletion of the fundamental beam.

XII. Common Experimental Techniques and Applications

There are a variety of experimental methods for determining the characteristics (magnitude, response time, spectrum, etc.) of $\chi^{(3)}$ (or $\chi^{(3)}_{\text{eff}}$). The merit of a technique depends on the nature of the nonlinearity and/or the specific property that we wish to measure. An example is obtaining short time resolution at the expense of sensitivity. Nonlinear optical coefficients can be determined absolutely or relative to a reference material. In the former case, accuracy is determined by the ability to precisely characterize the incident beams. There are many potential sources of error and misinterpretation in nonlinear optical measurements. In “thick” samples, for example, the phase shift that occurs during beam propagation can lead to varying irradiance at different points within the sample. This can be quite difficult to account for and properly model. It is usually best to work in the “external self action” regime, i.e. thin-sample limit so that beam propagation effects can be ignored [91](see also Section III). This greatly simplifies data analysis since the equation describing nonlinear absorption can be separated from nonlinear refraction. Even if the thin-sample approximation is satisfied, nonlinear refraction can deflect light so strongly *after* the sample that the detector does not collect all the transmitted energy. This will lead to an overestimation of the nonlinear loss. Particular care must be exercised when using

ultrashort pulses. Pulse broadening effects due to group velocity dispersion, for example, may cast ambiguity on the magnitude as well as response time associated with a nonlinearity.

We briefly discuss a few of the commonly used experimental methods: four-wave mixing, excite-probe techniques, interferometry, and Z-scan. It is practically impossible for any single technique to unambiguously separate the different nonlinear responses. Experiments are generally sensitive to several different nonlinearities at once. Different measurements are usually required to unravel the underlying physics, by varying parameters such as irradiance and pulsewidth. Near instantaneous nonlinearities such as two-photon absorption and the optical Kerr effect should be independent of pulsewidth. Slower nonlinear responses will change as the pulsewidth approaches the response time. Ultrafast and cumulative nonlinearities are often present simultaneously in experiments (e.g. semiconductors), thus hindering their experimental isolation

- ***Time Resolved Excite-Probe Techniques***

Pump-probe (excite-probe) measurements allow the study of temporal dynamics in nonlinear absorption [60] [27]. In the usual implementation, a relatively strong pump pulse excites the sample and changes its optical properties (Fig. 10). A weaker probe pulse interrogates the excitation region and detects changes. By varying the relative time separation of the two pulses, i.e. by appropriately advancing and delaying the probe pulse, the temporal response can be mapped out. Specifically, relatively slow and fast nonlinear responses can be identified. Often, but not always, the probe is derived from the excitation beam. In degenerate pump-probe (identical frequencies), the probe beam is isolated from the pump beam in a non-collinear geometry (i.e. spatial separation as in Fig. 10) or by orienting the probe with a different polarization (see Volume II, Chapter 14, “Ultrashort Laser Sources”).

Nondegenerate nonlinear absorption spectra can also be measured; one approach is to use a fixed frequency laser pump and continuum (white light) probe such as the output of a flashlamp [97]. The temporal width of a flashlamp source is usually much longer than the laser pulse, which causes a convolution of the fast two-photon response with much longer-lived cumulative nonlinearities in the probe spectrum. The availability of femtosecond white-light continuum sources has allowed nondegenerate spectra to be obtained on short time scales where the ultrafast response dominates [98] [27].

Interpretation of the nonlinear response is complicated by the fact that pump-probe experimental methods are sensitive to any and all induced change in transmission (or reflection); pump-induced phase shifts on the probe are not readily detected. A time-resolved technique that is very sensitive to index changes is the optical Kerr-gate. This is a form of the pump-probe experiment where induced anisotropy in a time-gated crystal leads to polarization changes [99]. Beyond the two-beam pump probe, three-beam interactions can produce a fourth beam through NLA and/or NLR. This is known as four-wave mixing and is discussed in the next section. The development of high irradiance, femtosecond pulsed laser systems has led to the evolution of pump-probe measurements that automatically yield the nondegenerate nonlinear absorption spectrum. The femtosecond pulse is split into two beams: one beam is used for sample excitation while the other beam is focused into an appropriate material to produce a white-light continuum for probing. This white-light continuum is used to measure the response over a range of frequencies ω' ; this data is suitable for numerical evaluation via the K-K integral in Eq. (23). For a sufficiently broad spectrum of data, the K-K integration yields the nondegenerate n_2 coefficient [100].

- ***Four-Wave Mixing***

The most general case of third-order interaction has all four interacting waves (three input and one scattered) at different frequencies. Generating and phase-matching three different laser wavelengths in an experiment is a formidable task; the benefit is often an improved signal-to-noise ratio.

The other extreme is when all four waves have identical frequency, a situation known as degenerate four-wave mixing (DFWM), although it is commonly (and less precisely) referred to as four-wave mixing (Volume II, Chapters 36, "Optical Properties of Semiconductors"; Volume II, Chapter 39, "Photorefractive Materials and Devices"). DFWM is readily implemented in the laboratory since only a single laser source is needed. There are two general cases: non-resonant and resonant DFWM. In transparent media (i.e. non-resonant) the index of refraction is usually a linear function of laser irradiance and non-resonant DFWM (wavelength far from an absorption resonance) leads to optical phase conjugation. Phase conjugation by the optical Kerr effect (Sec. V) is one of the most important applications involving third-order nonlinearities [26]. Non-resonant DFWM leads to the formation of a phase grating due the spatial modulation of the refractive index. Two of the beams "write" the phase grating while a third "reads" or probes the grating by diffracting from it, thereby generating a fourth beam (see Fig. 11). The diffracted beam can be either transmitted or reflected (i.e. a phase conjugate beam) from the material in a direction determined by the wave vectors of the interacting photons. In some experiments, the writing beams also serve to read the grating. One of the difficulties interpreting DFWM data for third-order nonlinearities is that the signal is proportional to $|\chi^{(3)}|^2 = |\Re\{\chi^{(3)}\} + \Im\{\chi^{(3)}\}|^2$, i.e. NLA and NLR both contribute. Separating the effects is difficult without performing additional experiments. Techniques that study different polarizations can provide information on the symmetry properties of $\chi^{(3)}$.

In resonant DFWM, there is the added complication of optical absorption at the frequency of the interacting light beams [101]. This is an example of a cascaded $\chi^{(1)}:\chi^{(1)}$ effective third-order nonlinearity discussed in Section IX, where absorption causes population in excited states resulting in a spatial grating due the spatial modulation of population. In principle, both phase and absorption gratings are present in resonant DFWM. In practice, it is usually the intensity-dependent changes of population (i.e. effective $\chi^{(3)}$) that dominate the nonlinear polarization although this is not always the case [76]. For example, photocarrier generation in a semiconductor can alter the bulk plasma frequency and thus modulate the refractive index, leading to a strong phase grating (see Section IX).

The diffracted beam contains a wealth of information about the system under study. In non-resonant DFWM, the absolute magnitude and spectral width of the Kerr-effect nonlinearity (n_2) can be obtained. Even more can be deduced from time-resolved DFWM, where the interacting beams are short laser pulses. If the pulses (two and sometimes three separate pulses) are delayed with respect to each other, the dynamic response of the nonlinear polarization can be measured. In resonant DFWM, the diffracted beam measures the coherent response of the optically coupled eigenstates of the system. The linewidth of the diffracted beam indicates the rate at which various physical processes broaden the transition. The nonlinear polarization can be washed out by mechanisms such as population relaxation and diffusion and scattering events associated with optically coupled states. Because of selection rules linking resonant states, various polarization geometries can be employed to study specific transitions. This can be very useful in studies of a complex system such as a semiconductor. Time-resolved experiments with short pulses provide

information that complements and elucidates spectral linewidth data obtained from measurements with long duration or continuous laser beams [26, 60, 102].

- ***Interferometry***

Interferometric methods can be used to measure nonlinearly induced phase distortion [103, 104]. One implementation of this approach places a sample in one path (e.g. arm) of an interferometer and the interference fringes are monitored as a function of irradiance. If the interferometer is set up to give a series of straight-line interference fringes for low input irradiance (linear regime), the fringes become curved near the region of high irradiance, such as the center of a Gaussian beam. The addition of a streak camera can add time resolution [27]. Alternatively, a third beam can be added to the experiment. The sample is in the path of one weak beam and the strong third beam. The fringe pattern of the two weak beams is monitored as a function of sample irradiance provided by the strong beam. The relative fringe shift observed when the strong beam is present and blocked gives the optical path length change. The nonlinear phase shift can thus be determined. Interferometric experiments require excellent stability and precise alignment. When these conditions are met, sensitivities of better than $\lambda/10^4$ induced optical path length change can be measured.

- ***Z-Scan***

The Z-scan was developed to measure the magnitude and sign of nonlinear refraction (NLR). It is also useful for characterizing nonlinear absorption (NLA) and separating the effects of NLR from NLA [105, 106]. The essential geometry is shown in Fig. 12. Using a single, focused laser beam, one measures the transmittance of a sample through a partially obscuring circular aperture (Z-scan) or around a partially obscuring disk (EZ-scan [107]) placed in the far field. The transmittance is determined as a function of the sample position (Z) measured with respect to the focal plane. Employing a Gaussian spatial profile beam simplifies the analysis.

We illustrate how Z-scan (or EZ-scan) data is related to the NLR of a sample. Assume, for example, a material with a positive nonlinear refractive index. We start the Z-scan far from the focus at a large value of negative Z (i.e. close to the lens). The beam irradiance is low and negligible NLR occurs; the transmittance remains relatively constant near this sample position. The transmittance is normalized to unity in this linear regime as depicted in Fig. 13. As the sample is brought closer to focus, the beam irradiance increases leading to self-focusing. This positive NLR moves the focal point closer to the lens causing greater beam divergence in the far field. Transmittance through the aperture is reduced. As the sample is moved past the focus, self-focusing increasingly collimates the beam resulting in enhanced transmittance through the aperture. Translating the sample further toward the detector reduces the irradiance to the linear regime and returns the normalized transmittance to unity. Reading the data right to left, a valley followed by peak is indicative of positive NLR. In negative NLR, one finds exactly the opposite: a peak followed by a valley. This is due to laser-induced self-defocusing. Characteristic curves for both types of NLR are shown in Fig. 12. The EZ-scan reverses the peak and valley in both cases. In the far field, the largest fractional changes in irradiance occur in the wings of a Gaussian beam. For this reason, the EZ-scan can be more than an order-of-magnitude more sensitive than the Z-scan.

We define an easily measurable quantity ΔT_{pv} as the difference between the normalized peak and valley transmittance: $T_p - T_v$. Analysis shows that variation of ΔT_{pv} is linearly-dependent on the

temporally averaged induced phase distortion, defined here as $\Delta\Phi_0$. If the Z-scan aperture is closed to allow linear transmission of less than 10 percent, and $\Delta T_{pv} < 1$ [105, 108]

$$\Delta T_{pv} \cong 0.41 |\Delta\Phi_0|, \quad (48)$$

assuming cw illumination. If the experiment is capable of resolving transmission changes $\Delta T_{pv} \cong 1\%$, the Z-scan will be sensitive to wavefront distortion of less than $\lambda/250$ (i.e., $\Delta\Phi_0 = 2\pi/250$). The Z-scan has demonstrated sensitivity to a nonlinearly induced optical path length change of nearly $\lambda/10^3$ while the EZ-scan has shown a sensitivity of $\lambda/10^4$, including temporal averaging over the pulsewidth.

To this point in the discussion, we have assumed a purely refractive nonlinearity with no NLA. It has been shown that two-photon absorption will suppress the peak and enhance the valley. If NLA and NLR are present simultaneously, a numerical fitting procedure can extract both the nonlinear refractive and absorptive coefficients. Alternatively, a second Z-scan with the aperture removed (all the transmitted light collected) can independently determine the NLA. Considering 2PA only and a Gaussian input beam, the Z-scan traces out a symmetric Lorentzian shape. The so-called open aperture Z-scan is sensitive *only* to NLA. One can then divide the partially obscuring Z-scan data by the open aperture data to give a curve that shows only nonlinear refraction. By performing these two types of Z-scans, we can isolate NLR and NLA without the need for a complicated numerical analysis of a single data set obtained with an aperture.

- ***All-optical switching and optical bistability***

Since the early 1980's, there has been substantial interest in third-order nonlinear optical behavior in materials because of the potential for performing high-speed switching operations – gate speeds many orders of magnitude faster than conventional electronics have been demonstrated. The possibility of increasing data rates on information networks provides the obvious motivation for this research. A bistable optical switch has two stable output states for a given input, i.e. a specific optical power level. This has implications for applications such as optical data storage and power limiting. Both non-resonant $\chi^{(3)}$ and resonant “effective” $\chi^{(3)}$ processes have been extensively studied, primarily in semiconductors. The early work looked at bulk semiconductor behavior, but as the technology matured the emphasis shifted to specially designed optical waveguides made from suitable material. At the time of this writing, both resonant and non-resonant approaches have encountered problems that have limited practical use. The bound electronic nonlinearity responds on a femtosecond timescale but is inherently weak. The laser irradiance must be increased to compensate, but this leads to the unwelcome presence of 2PA and associated losses. Resonant nonlinearities must involve the generation of carriers (electrons and holes). While such nonlinearities can be exceptionally strong, the speed of an optical switch depends crucially on the ability to manipulate the carriers. Generation of electron-hole pairs, for example, may dramatically affect the refractive index of a semiconductor and its ability to modulate light, but if the carriers have a long recombination lifetime the switch recovery time will be relatively slow. Other significant issues that must be weighed when comparing optical switching schemes to the all-electronic approach (i.e. transistors and integrated circuits) include device packaging density and heat removal [18, 42, 53, 72, 109, 110]. For more detailed discussion, consult the chapter in this volume on “all-optical-switching”.

XIII. References

- [1] N. Bloembergen, *Nonlinear optics*. Redwood City, Calif.: Addison-Wesley Pub. Co., 1992.
- [2] S. A. Akhmanov and R. V. Khokhlov, *Problems of nonlinear optics; electromagnetic waves in nonlinear dispersive media*. New York, : Gordon and Breach Science Publishers, 1972.
- [3] R. W. Boyd, *Nonlinear optics*. Boston: Academic Press, 1992.
- [4] P. N. Butcher and D. Cotter, *The elements of nonlinear optics*. Cambridge ; New York: Cambridge University Press, 1990.
- [5] G. P. Agrawal, *Nonlinear fiber optics*, 2nd ed. San Diego: Academic Press, 1995.
- [6] W. Demtröder, M. Inguscio, and North Atlantic Treaty Organization. Scientific Affairs Division., *Applied laser spectroscopy*. New York: Plenum Press, 1990.
- [7] D. C. Hanna, M. A. Yuratich, and D. Cotter, *Nonlinear optics of free atoms and molecules*. Berlin ; New York: Springer-Verlag, 1979.
- [8] F. A. Hopf and G. I. Stegeman, *Applied classical electrodynamics*, Reprint ed. Malabar, FL: Krieger Pub. Co., 1992.
- [9] I.-C. Khoo, J.-F. Lam, and F. Simoni, *Nonlinear optics and optical physics*. Singapore ; River Edge, NJ: World Scientific, 1994.
- [10] V. S. Letokhov and V. P. Chebotayev, *Nonlinear laser spectroscopy*. Berlin ; New York: Springer-Verlag, 1977.
- [11] M. D. Levenson and S. Kano, *Introduction to nonlinear laser spectroscopy*, Rev. ed. Boston: Academic Press, 1988.
- [12] S. R. Marder, J. E. Sohn, G. D. Stucky, American Chemical Society. Division of Organic Chemistry., American Chemical Society. Division of Inorganic Chemistry., and American Chemical Society. Meeting, *Materials for nonlinear optics : chemical perspectives*. Washington, DC: American Chemical Society, 1991.
- [13] D. L. Mills, *Nonlinear optics : basic concepts*, 2nd, enl. ed. New York: Springer, 1998.
- [14] A. C. Newell and J. V. Moloney, *Nonlinear optics*. Redwood City, Calif.: Addison-Wesley, 1992.
- [15] E. G. Sauter, *Nonlinear optics*. New York: Wiley, 1996.
- [16] M. Schubert and B. Wilhelmi, *Nonlinear optics and quantum electronics*. New York: Wiley, 1986.
- [17] Y. R. Shen, *The principles of nonlinear optics*. New York: J. Wiley, 1984.
- [18] R. L. Sutherland, *Handbook of nonlinear optics*. New York: Marcel Dekker, 1996.
- [19] P. Yeh, *Nonlinear optics and applications*, vol. 613. Bellingham: Society of Photo-Optical Instrumentation Engineers, 1986.
- [20] P. Yeh, *Introduction to photorefractive nonlinear optics*. New York: Wiley, 1993.
- [21] F. Zernike and J. E. Midwinter, *Applied nonlinear optics*. New York, : Wiley, 1973.

- [22] B. E. A. Saleh and M. C. Teich, *Fundamentals of photonics*. New York: Wiley, 1991.
- [23] A. Yariv, *Optical electronics in modern communications*, 5th ed. New York: Oxford University Press, 1997.
- [24] A. Yariv, *Quantum electronics*, 3rd ed. New York: Wiley, 1989.
- [25] A. Yariv and P. Yeh, *Optical waves in crystals : propagation and control of laser radiation*. New York: Wiley, 1984.
- [26] R. A. Fisher, *Optical phase conjugation*. New York, N.Y.: Academic Press, 1983.
- [27] J.-C. Diels and W. Rudolph, *Ultrashort laser pulse phenomena : fundamentals, techniques, and applications on a femtosecond time scale*. San Diego: Academic Press, 1996.
- [28] B. I. A. Zel'dovich, N. F. Pilipetskii, and V. V. Shkunov, *Principles of phase conjugation*. Berlin ; New York: Springer-Verlag, 1985.
- [29] B. S. Wherrett and P. G. Harper, "Nonlinear Optics," . London: Academic Press, 1977.
- [30] E. Garmire and A. Kost, "Nonlinear Optics in Semiconductors I & II," in *Semiconductors and Semimetals*, vol. 58, R. K. Wilardson and E. R. Webber, Eds.: Academic Press, 1999.
- [31] M. Sheik-Bahae and E. W. Van Stryland, "Optical nonlinearities in the transparency region of bulk semiconductors," in *Nonlinear Optics in Semiconductors I*, vol. 58, *Semiconductors and Semimetals*, E. Garmire and A. Kost, Eds.: Academic Press, 1999, pp. 257-318.
- [32] E. W. Van Stryland, A. L. Smirl, T. F. Boggess, M. J. Soileau, B. S. Wherrett, and F. Hopf, "Weak-Wave Retardation and Phase-Conjugate Self-Defocusing in Si," in *Picosecond Phenomena III*, R. M. H. K.B. Eissenthal, W. Kaiser, and A. Laubereau, Ed.: Springer-Verlag,, 1982.
- [33] J. S. Toll, "Casaulity and dispersion relation: Logical foundation," *Phys. Rev.*, vol. 104, pp. 1760-1770, 1956.
- [34] H. M. Nussenzveig, *Causality and dispersion relations*. New York,: Academic Press, 1972.
- [35] P. J. Caspers, "Dispersion relations for nonlinear response," *Phys. Rev. A*, vol. 133, pp. 1249, 1964.
- [36] S. M. Kogan, "On the electromagnetics of weakly nonlinear media," *Sov. Phys. JETP*, vol. 16, pp. 217, 1963.
- [37] P. J. Price, "Theory of Quadratic Response Functions," *Phys. Rev.*, vol. 130, pp. 1792, 1964.
- [38] F. L. J. Ridener and R. H. J. Good, "Dispersion Relations for Nonlinear Systems or Arbitrary Degree," *Phys. Rev. B*, vol. 11, pp. 2768, 1975.
- [39] D. C. Hutchings, M. Sheik-Bahae, D. J. Hagan, and E. W. Van Stryland, "Kramers-Kronig Relations in Nonlinear Optics," *Optical and Quantum Electronics*, vol. 24, pp. 1-30, 1992.
- [40] F. Bassani and S. Scandolo, "Dispersion-Relations and Sum-Rules in Nonlinear Optics," *Phys. Rev. B-Condensed Matter*, vol. 44, pp. 8446-8453, 1991.

- [41] D. A. B. Miller, C. T. Seaton, M. E. Prise, and S. D. Smith, "Band-Gap-Resonant Non-Linear Refraction in Iii-V Semiconductors," *Phys. Rev. Lett.*, vol. 47, pp. 197-200, 1981.
- [42] B. S. Wherrett, A. C. Walker, and F. A. P. Tooley, "Nonlinear refraction for cw optical bistability," in *Optical nonlinearities and instabilities in semiconductors*, H. Haug, Ed. Boston: Academic Press, 1988, pp. xi, 440.
- [43] M. Sheik-Bahae, D. J. Hagan, and E. W. Van Stryland, "Dispersion and Band-Gap Scaling of the Electronic Kerr Effect in Solids Associated With 2-Photon Absorption," *Phys. Rev. Lett.*, vol. 65, pp. 96-99, 1990.
- [44] M. Sheik-Bahae, D. C. Hutchings, D. J. Hagan, and E. W. Van Stryland, "Dispersion of Bound Electronic Nonlinear Refraction in Solids," *IEEE J. Quantum Electron.*, vol. 27, pp. 1296-1309, 1991.
- [45] M. Sheik-Bahae, "Nonlinear optics of bound electrons in solids," in *Nonlinear optical materials*, J. V. Moloney, Ed. New York: Springer, 1998, pp. xi, 245.
- [46] D. J. Moss, E. Ghahramani, J. E. Sipe, and H. M. Van Driel, "Band-Structure Calculation of Dispersion and Anisotropy in $\chi^{(3)}$ For 3rd-Harmonic Generation in Si, Ge, and GaAs," *Phys. Rev. B*, vol. 41, pp. 1542-1560, 1990.
- [47] R. Adair, L. L. Chase, and S. A. Payne, "Nonlinear Refractive-Index Measurements of Glasses Using 3-Wave Frequency Mixing," *Journal of the Optical Society of America B-Optical Physics*, vol. 4, pp. 875-881, 1987.
- [48] R. Adair, L. L. Chase, and S. A. Payne, "Nonlinear Refractive-Index of Optical-Crystals," *Phys. Rev. B-Condensed Matter*, vol. 39, pp. 3337-3350, 1989.
- [49] S. R. Friberg, A. M. Weiner, Y. Silberberg, B. G. Sfez, and P. S. Smith, "Femtosecond Switching in a Dual-Core-Fiber Nonlinear Coupler," *Opt. Lett.*, vol. 13, pp. 904-906, 1988.
- [50] M. J. Weber, D. Milam, and W. L. Smith, "Non-Linear Refractive-Index of Glasses and Crystals," *Optical Engineering*, vol. 17, pp. 463-469, 1978.
- [51] L. F. Mollenauer, R. H. Stolen, and J. P. Gordon, *Phys. Rev. Lett.*, vol. 45, pp. 1095, 1980.
- [52] D. E. Spence, P. N. Kean, and W. Sibbett, "60-Fsec Pulse Generation From a Self-Mode-Locked Ti-Sapphire Laser," *Optics Letters*, vol. 16, pp. 42-44, 1991.
- [53] H. M. Gibbs, *Optical bistability : controlling light with light*. Orlando: Academic Press, 1985.
- [54] M. N. Islam, *Ultrafast fiber switching devices and systems*. Cambridge England ; New York, NY, USA: Cambridge University Press, 1992.
- [55] N. L. Boling, A. J. Glass, and A. Owyong, "Empirical relationships for predicting nonlinear refractive index changes in optical solids," *IEEE J. Quantum Electron.*, vol. QE-14, pp. 601, 1978.
- [56] P. P. Ho and R. R. Alfano, "Optical Kerr Effect in Liquids," *Phys. Rev. A*, vol. 20, pp. 2170, 1979.
- [57] F. A. Hopf and G. I. Stegeman, *Applied classical electrodynamics*. New York: Wiley, 1985.

- [58] J. F. Reintjes, *Nonlinear optical parametric processes in liquids and gases*. New York: Academic Press, 1984.
- [59] M. D. Levenson, *Introduction to nonlinear laser spectroscopy*. New York: Academic Press, 1982.
- [60] W. Kaiser and D. H. Auston, *Ultrashort laser pulses : generation and applications*, 2nd ed. Berlin ; New York: Springer, 1993.
- [61] M. Cardona and G. Güntherodt, *Light scattering in solids VI : recent results, including high-Tc superconductivity*. Berlin ; New York: Springer-Verlag, 1991.
- [62] J. J. Valentini, "Laser Raman Techniques," in *Optical Engineering: Laser Spectroscopy and its Applications*, vol. 11, L. J. Radziemski, R. W. Solarz, and J. A. Paisner, Eds. NY: Dekker, 1987.
- [63] D. A. Long, *Raman Spectroscopy*. NY: McGraw-Hill,, 1977.
- [64] G. L. Eesley, *Cohernet Raman Spectroscopy*. Oxford: Pergamon, 1981.
- [65] L. A. Woodward, "Raman Spectroscopy: Theory and Practice," , H. A. Szymanski, Ed. NY: Plenum, 1987.
- [66] E. W. Van Stryland and L. Chase, "Two-photon absorption: Inorganic Materials," in *Handbook of Laser Science and Technology, Supplement 2, Optical Materials*, M. Weber, Ed.: CRC Press, 1994, pp. 299-328.
- [67] E. W. Van Stryland, H. Vanherzeele, M. A. Woodall, M. J. Soileau, A. L. Smirl, S. Guha, and T. F. Boggess, "2 Photon-Absorption ; Nonlinear Refraction ; and Optical Limiting in Semiconductors," *Optical Engineering*, vol. 24, pp. 613-623, 1985.
- [68] E. W. Van Stryland, M. A. Woodall, H. Vanherzeele, and M. J. Soileau, "Energy Band-Gap Dependence of 2-Photon Absorption," *Opt. Lett.*, vol. 10, pp. 490-492, 1985.
- [69] B. S. Wherrett, "Scaling Rules For Multiphoton Interband Absorption in Semiconductors," *Journal of the Optical Society of America B-Optical Physics*, vol. 1, pp. 67-72, 1984.
- [70] J. I. Pankove, *Optical Processes in Semiconductors*. New York: Dover, 1971.
- [71] C. Kittel, *Introduction to solid state physics*, 7th ed. New York: Wiley, 1996.
- [72] A. Miller, D. A. B. Miller, and S. D. Smith, "Dynamic Non-Linear Optical Processes in Semiconductors," *Advances in Physics*, vol. 30, pp. 697-800, 1981.
- [73] H. Haug and S. W. Koch, *Quantum theory of the optical and electronic properties of semiconductors*, 3rd ed. Singapore: World Scientific, 1994.
- [74] W. W. Chow, S. W. Koch, and M. Sargent, *Semiconductor-laser physics*, Corrected printing ed. Berlin ; New York: Springer-Verlag, 1997.
- [75] L. Banyai and S. W. Koch, "A Simple Theory For the Effects of Plasma Screening On the Optical-Spectra of Highly Excited Semiconductors," *Zeitschrift Fur Physik B-Condensed Matter*, vol. 63, pp. 283-291, 1986.
- [76] R. K. Jain and M. B. Klein, "Degenerate Four-Wave Mixing in Semiconductors," in *Optical Phase Conjugation*, R. A. Fisher, Ed. New York, N.Y.: Academic Press, 1983.
- [77] J. I. Steinfeld, *Laser and coherence spectroscopy*. New York: Plenum Press, 1978.

- [78] M. Sargent, M. O. Scully, and W. E. Lamb, *Laser physics*. Reading, Mass. ; London: Addison-Wesley, 1977.
- [79] J. Feinberg, "Optical Phase Conjugation in Photorefractive Materials," in *Optical Phase Conjugation*, R. A. Fisher, Ed. New York, N.Y.: Academic Press, 1983.
- [80] J. E. Millard, M. Ziari, and A. Partovi, "Photorefractivity in semiconductors," in *Nonlinear Optics in Semiconductors I*, vol. 58, *Semiconductors and Semimetals*, E. Garmire and A. Kost, Eds.: Academic Press, 1999.
- [81] R. DeSalvo, D. J. Hagan, M. Sheik-Bahae, G. Stegeman, E. W. Van Stryland, and H. Vanherzeele, "Self-Focusing and Self-Defocusing By Cascaded 2nd-Order Effects in Ktp," *Opt. Lett.*, vol. 17, pp. 28-30, 1992.
- [82] N. R. Belashenkov, S. V. Gagarskii, and M. V. Inochkin, "Nonlinear refraction of light on second-harmonic generation," *Opt. Spektrosk.*, vol. 66, pp. 1383-1386, 1989.
- [83] G. I. Stegeman, M. Sheik-Bahae, E. Van Stryland, and G. Assanto, "Large Nonlinear Phase-Shifts in 2nd-Order Nonlinear-Optical Processes," *Opt. Lett.*, vol. 18, pp. 13-15, 1993.
- [84] E. W. Van Stryland, "Third-Order and Cascaded Nonlinearities," presented at Laser Sources and Applications, 1996.
- [85] G. Assanto, G. Stegeman, M. Sheik-Bahae, and E. Van Stryland, "All-Optical Switching Devices Based On Large Nonlinear Phase-Shifts From 2nd Harmonic-Generation," *Appl. Phys. Lett.*, vol. 62, pp. 1323-1325, 1993.
- [86] G. Assanto, G. I. Stegeman, M. Sheik-Bahae, and E. Van Stryland, "Coherent Interactions For All-Optical Signal-Processing Via Quadratic Nonlinearities," *IEEE J. Quantum Electron.*, vol. 31, pp. 673-681, 1995.
- [87] W. Torruellas, B. Lawrence, and G. I. Stegeman, "Self-Focusing and 2d Spatial Solitons in Pts," *Electronics Letters*, vol. 32, pp. 2092-2094, 1996.
- [88] W. E. Torruellas, Z. Wang, D. J. Hagan, E. W. Vanstryland, G. I. Stegeman, L. Torner, and C. R. Menyuk, "Observation of 2-Dimensional Spatial Solitary Waves in a Quadratic Medium," *Physical Review Letters*, vol. 74, pp. 5036-5039, 1995.
- [89] L. J. Qian, X. Liu, and F. W. Wise, "Femtosecond Kerr-lens mode locking with negative nonlinear phase shifts," *Optics Letters*, vol. 24, pp. 166-168, 1999.
- [90] M. Sheik-Bahae, A. A. Said, D. J. Hagan, M. J. Soileau, and E. W. Van Stryland, "Nonlinear Refraction and Optical Limiting in Thick Media," *Optical Engineering*, vol. 30, pp. 1228-1235, 1991.
- [91] A. E. Kaplan, "External Self-focusing of Light by a Nonlinear Layer," *Radiophys. Quantum Electron.*, vol. 12, pp. 692-696, 1969.
- [92] J. H. Marburger, in *Progress in Quantum Electronics*, J. H. Sanders and S. Stenholm, Eds. N.Y.: Pergamon Press, 1977.
- [93] H. A. Haus, J. G. Fujimoto, and E. P. Ippen, "Analytic Theory of Additive Pulse and Kerr Lens Mode-Locking," *IEEE J. Quantum Electron.*, vol. 28, pp. 2086-2096, 1992.
- [94] G. P. Agrawal, *Nonlinear fiber optics*. Boston: Academic Press, 1989.

- [95] A. Barthelemy, S. Maneuf, and C. Froehly, "Soliton Propagation and Self-Confinement of Laser-Beams By Kerr Optical Non-Linearity," *Optics Communications*, vol. 55, pp. 201-206, 1985.
- [96] S. Maneuf, A. Barthelemy, and C. Froehly, "Soliton Beam Propagation : Space-Time Behavior and Spectral Features," *Journal of Optics*, vol. 17, pp. 139-145, 1986.
- [97] J. J. Hopfield, J. M. Worlock, and K. Park, "Two-Quantum Absorption Spectrum of KI," *Phys. Rev. Lett.*, vol. 11, pp. 414, 1963.
- [98] J. A. Bolger, A. K. Kar, B. S. Wherrett, R. Desalvo, D. C. Hutchings, and D. J. Hagan, "Nondegenerate 2-Photon Absorption-Spectra of Znse ; Zns and Zno," *Optics Communications*, vol. 97, pp. 203-209, 1993.
- [99] P. Maker, R. Terhune, and C. Savage, "Intensity-Dependent Changes in the Refractive Index of Liquids," *Phys. Rev. Lett.*, vol. 12, pp. 507, 1964.
- [100] D. J. Hagan, E. Miesak, R. Negres, S. Ross, J. Lim, and E. W. Van Stryland, "Nonlinear spectrometry of chromophores for optical limiting," *SPIE Proceedings*, vol. 3472, pp. 80-90, 1998.
- [101] R. L. Abrams, J. F. Lam, R. C. Lind, D. G. Steel, and P. F. Liao, "Phase Conjugation and High Resolution Spectroscopy by Resonant Degenerate Four-Wave Mixing," in *Optical Phase Conjugation*, R. A. Fisher, Ed. New York, N.Y.: Academic Press, 1983.
- [102] J. Shah, *Ultrafast spectroscopy of semiconductors and semiconductor nanostructures*. Berlin ; New York: Springer, 1996.
- [103] M. J. Weber, D. Milam, and W. L. Smith, "Nonlinear Refractive Index of Glasses and Crystals," *Opt. Eng.*, pp. 463, 1978.
- [104] M. J. Moran, C. Y. She, and R. L. Carmen, "Interferometric Measurements of the Nonlinear Refractive Index Coefficient Relative to CS₂ in the Laser System Related Materials,," *IEEE J. Quantum Electron.*, vol. 11, pp. 259, 1975.
- [105] M. Sheik-Bahae, A. A. Said, T. H. Wei, D. J. Hagan, and E. W. Van Stryland, "Sensitive Measurement of Optical Nonlinearities Using a Single Beam," *IEEE J. Quantum Electron.*, vol. 26, pp. 760-769, 1990.
- [106] E. W. Van Stryland and M. Sheik-Bahae, "Z-Scan," in *Characterization techniques and tabulations for organic nonlinear optical materials*, M. G. Kuzyk and C. W. Dirk, Eds. New York: Marcel Dekker, 1998, pp. xii, 894.
- [107] T. Xia, D. J. Hagan, M. Sheik-Bahae, and E. W. Van Stryland, "Eclipsing Z-Scan Measurement of Lambda/10(4) Wave-Front Distortion," *Opt. Lett.*, vol. 19, pp. 317-319, 1994.
- [108] M. Sheik-Bahae, A. A. Said, and E. W. Van Stryland, "High-Sensitivity ; Single-Beam N2 Measurements," *Opt. Lett.*, vol. 14, pp. 955-957, 1989.
- [109] G. Stegeman and E. Wright, "All-optical waveguide switching," *Optical and Quantum Electronics*, vol. 22, pp. 95, 1990.
- [110] G. I. Stegeman, A. Villeneuve, J. Kang, J. S. Aitchison, C. N. Ironside, K. Alhemyari, C. C. Yang, C. H. Lin, H. H. Lin, G. T. Kennedy, R. S. Grant, and W. Sibbett, "AlGaAs Below Half Bandgap : the Silicon of Nonlinear-Optical Materials," *International Journal of Nonlinear Optical Physics*, vol. 3, pp. 347-371, 1994.

XIV. Figure Captions

Fig. 1 Time-ordering sequences illustrating all possible third-order paths. Arrows depict photons. Note that in general, the size of the arrows can be different provided their vector sum is zero. The number of terms is obtained assuming emission of a photon at ω_4 . Arrows not marked for clarity.

Fig. 2 Energy level diagrams for some important third-order nonlinear optical processes: a) third-harmonic generation (THG); b) coherent anti-Stokes Raman scattering (CARS); c) two-photon absorption (2PA).

Fig. 3 Calculated dispersion of nonlinear absorption. Also shown is the two-photon absorption spectrum.

Fig. 4 Simple picture of CS₂ molecule

Fig. 5 Raman scattering

Fig. 6 Stimulated Raman processes

Fig. 7 Absorption saturation and refraction of a two level atomic system

Fig. 8 Cascaded $\chi^{(2)};\chi^{(2)}$ effective third-order nonlinearities

Fig. 9 Calculated phase shifts in cascaded $\chi^{(2)};\chi^{(2)}$

Fig. 10 Pump-probe experiment

Fig. 11 Schematic diagram of a four-wave mixing experiment

Fig. 12 Z-scan experimental arrangement

Fig. 13 Representative curves depicting nonlinear refraction (both positive and negative) as measured by the Z-scan

Table 1

| Nonlinear Process | $8P(\omega_4)/\epsilon_0\chi^{(3)}$ | ω_4 |
|--|---|--|
| <ul style="list-style-type: none"> • Third Harmonic Generation (THG) • Sum Frequency Generation (SFG) | $E_j^3 \quad j=1, \dots, 3$ $3E_i E_j^2$ $i, j=1, 2, 3 \quad i \neq j$ $6E_1 E_2 E_3$ | $3\omega_1, 3\omega_2, 3\omega_3$ $2\omega_1+\omega_2, 2\omega_1+\omega_3,$ $2\omega_2+\omega_3, 2\omega_2+\omega_1,$ $2\omega_3+\omega_1, 2\omega_3+\omega_2,$ $\omega_1+\omega_2+\omega_3$ |
| <ul style="list-style-type: none"> • Frequency Mixing • Parametric Amplification • Coherent Stokes and Anti-Stokes Raman Scattering (CSRS and CARS) | $3E_i^* E_j^2$ $i, j=1, 2, 3 \quad i \neq j$ $6E_i^* E_j E_k$ $i, j, k=1, 2, 3 \quad i \neq j \neq k$ $6E_i^* E_j^* E_k$ $i, j, k=1, 2, 3 \quad i \neq j \neq k$ | $2\omega_1-\omega_2, 2\omega_1-\omega_3,$ $2\omega_2-\omega_3, 2\omega_2-\omega_1,$ $2\omega_3-\omega_1, 2\omega_3-\omega_2,$ $\omega_1+\omega_2-\omega_3,$ $\omega_1-\omega_2+\omega_3,$ $-\omega_1+\omega_2+\omega_3$ $\omega_1-\omega_2-\omega_3,$ $-\omega_1-\omega_2+\omega_3,$ $-\omega_1+\omega_2-\omega_3$ |
| <ul style="list-style-type: none"> • Bound-Electronic Optical Kerr Effect • Raman Induced Kerr Effect (RIKE) • Molecular Orientational Kerr Effect • Two-Photon Absorption (2PA) • a.c.. Stark Effect • Stimulated Raman Scattering (SRS) • Stimulated Rayleigh-Wing Scattering | $3E_i^2 E_i^*$ $i=1, 2, 3$ $6E_i E_j E_j^*$ $i, j=1, 2, 3, \quad i \neq j$ | $\omega_1, \omega_2, \omega_3$ |

Figure 1

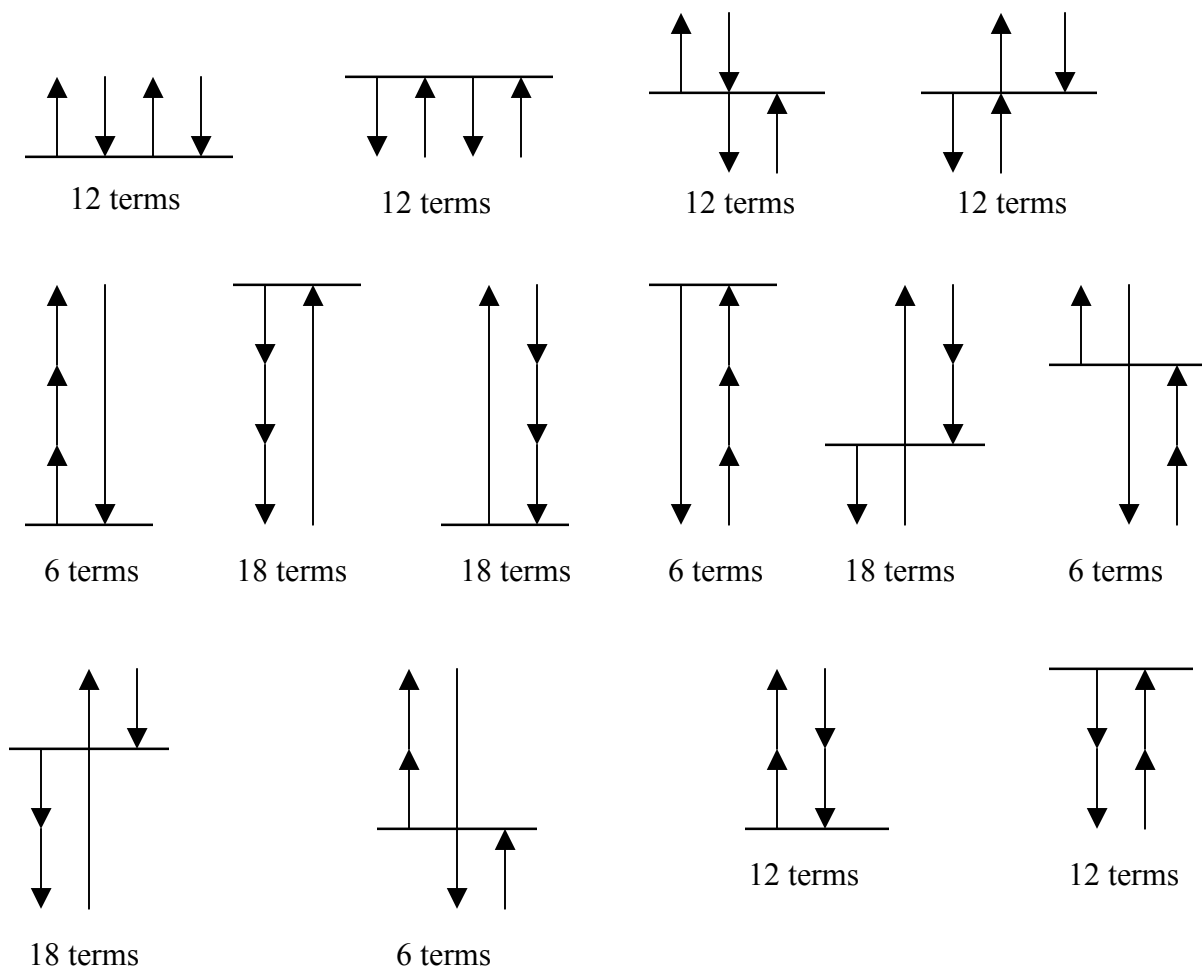


Figure 2

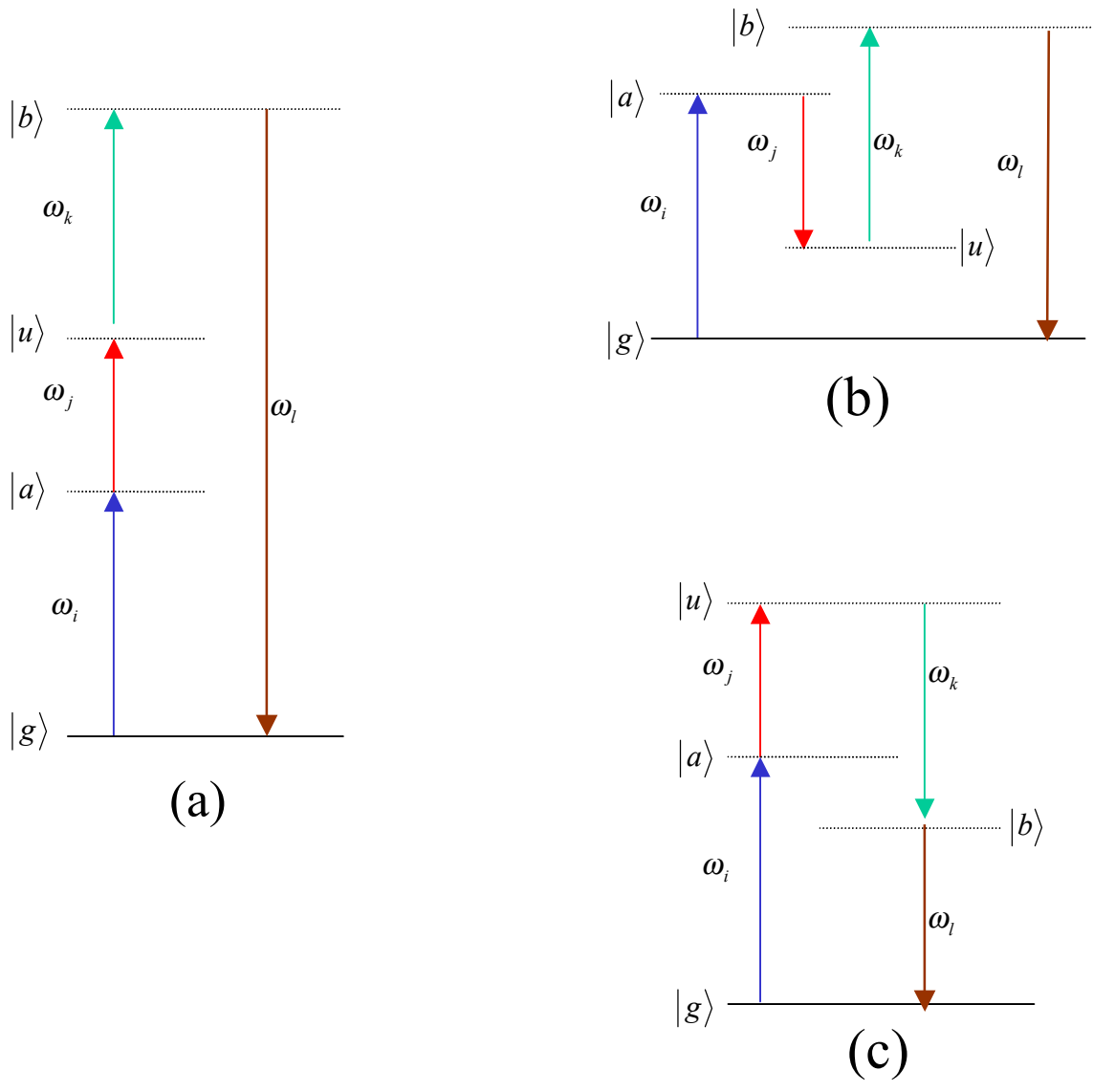


Figure 3

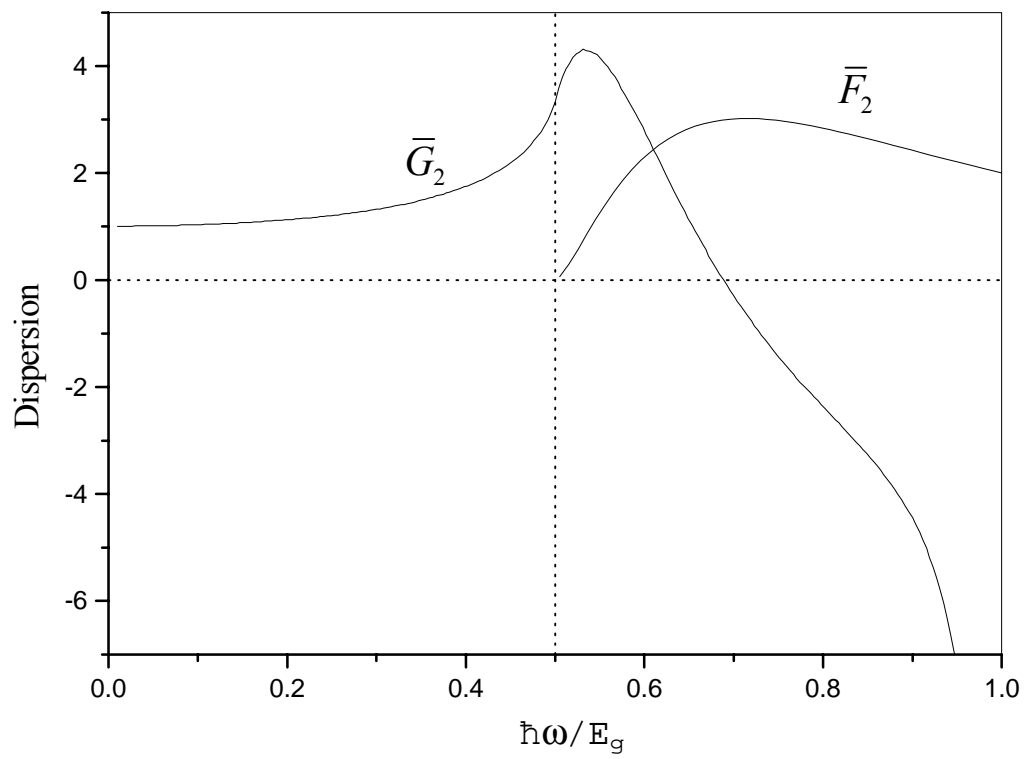


Figure 4

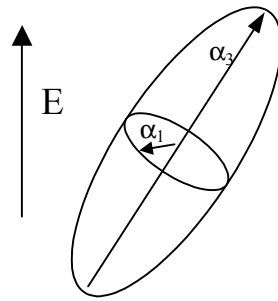
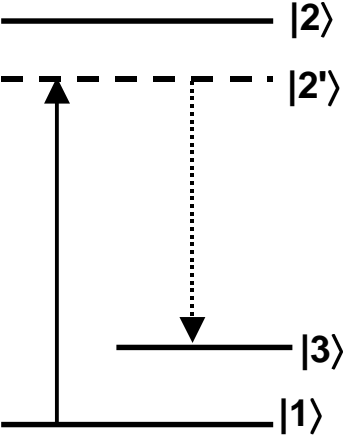


Figure 5

Stokes shifted
Raman scattering



Anti-Stokes shifted
Raman scattering

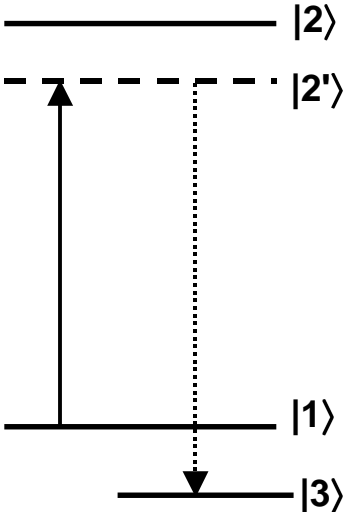


Figure 6

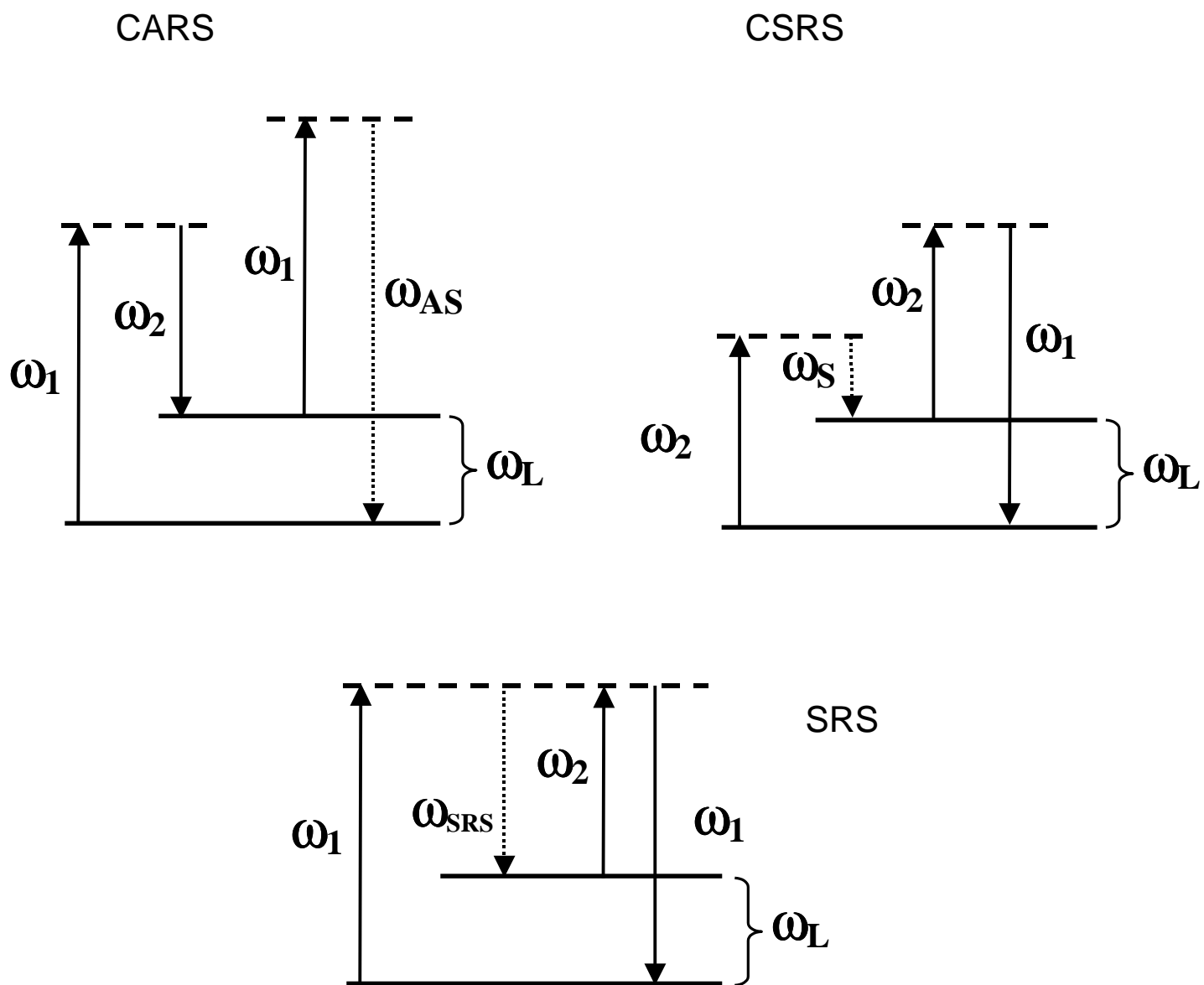


Figure 7

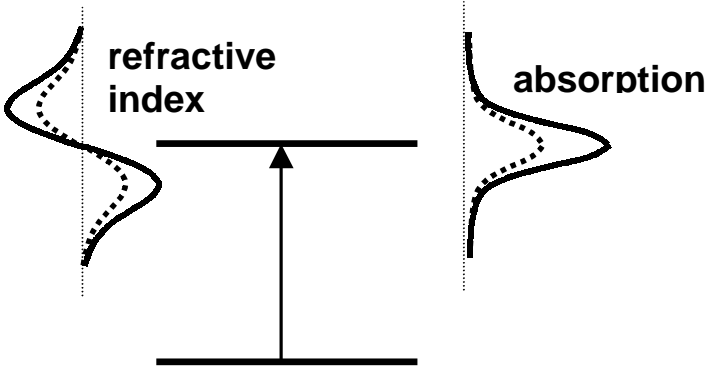


Figure 8

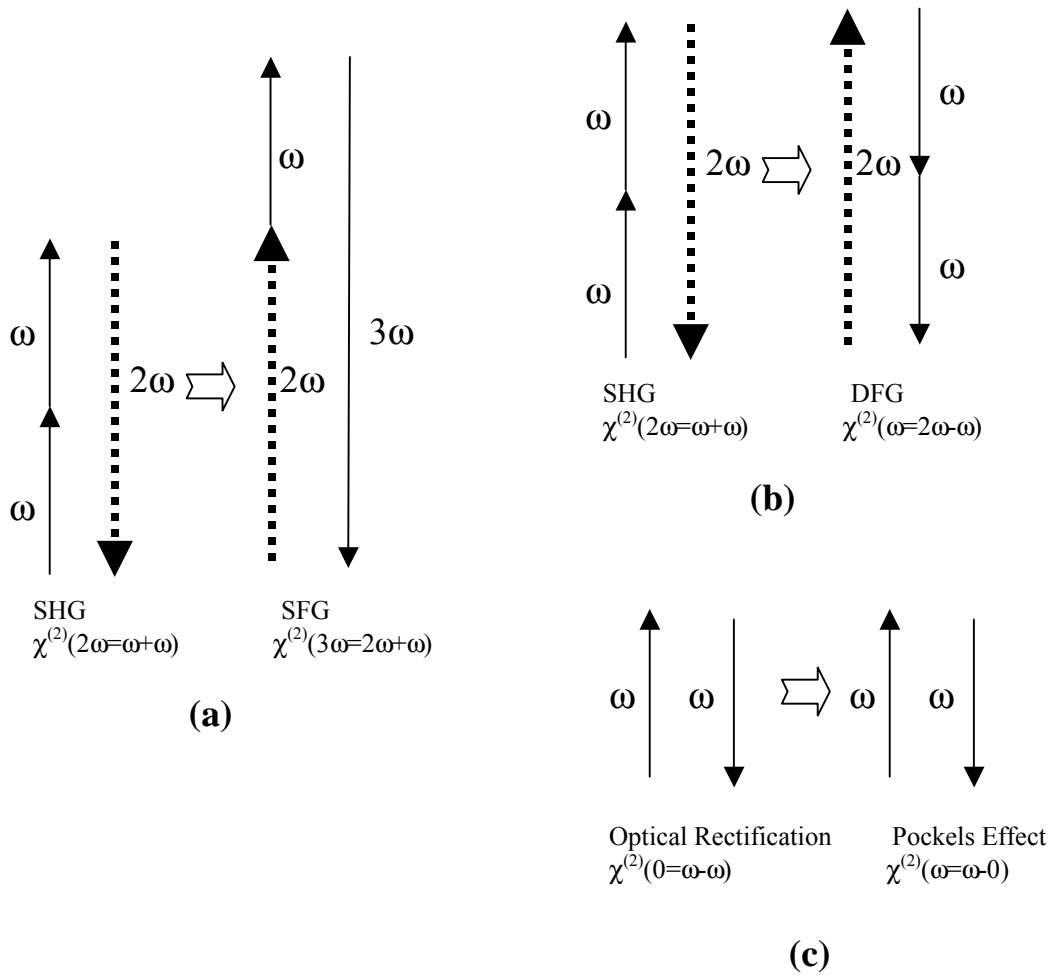


Figure 9

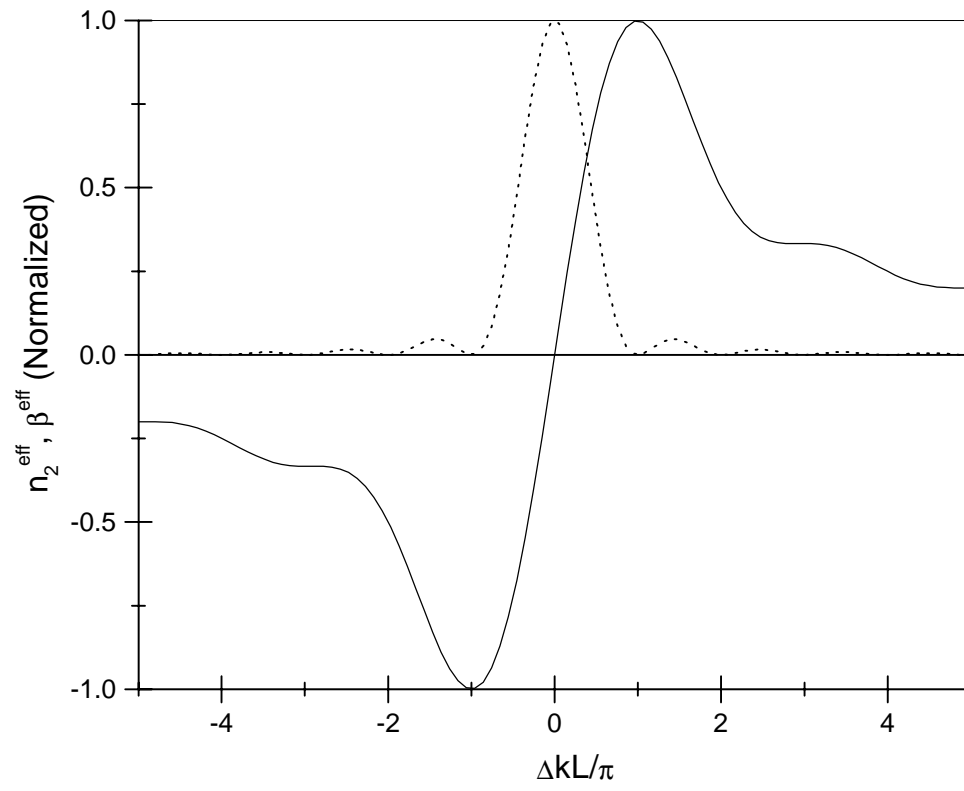


Figure 10

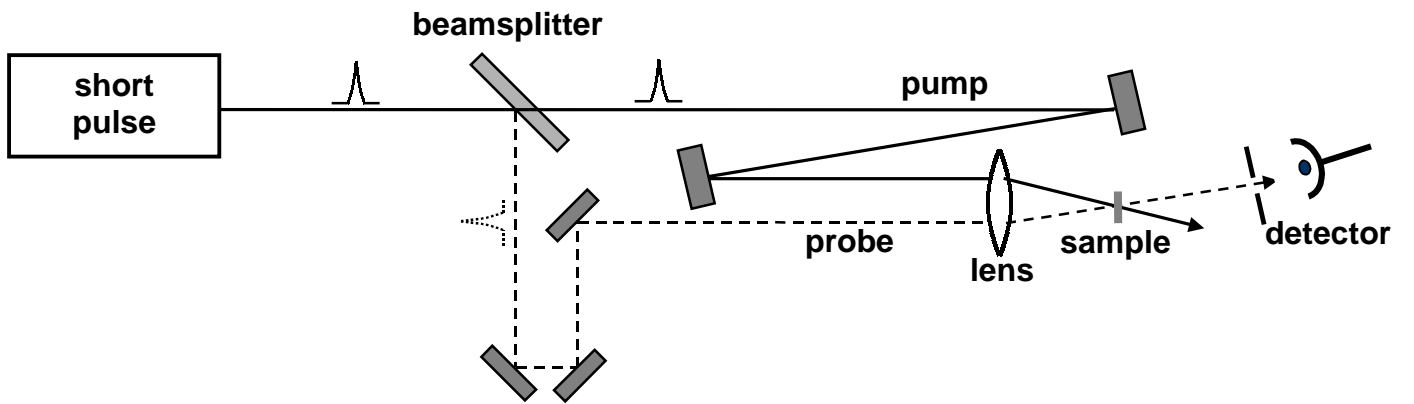


Fig. 11

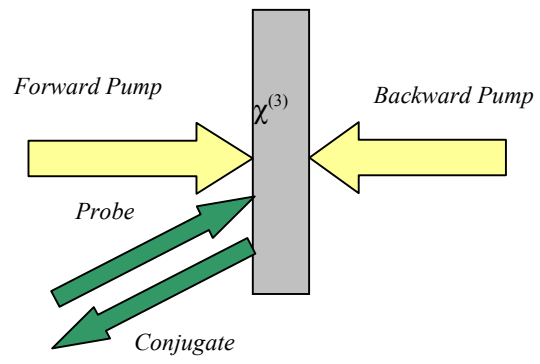


Figure 12

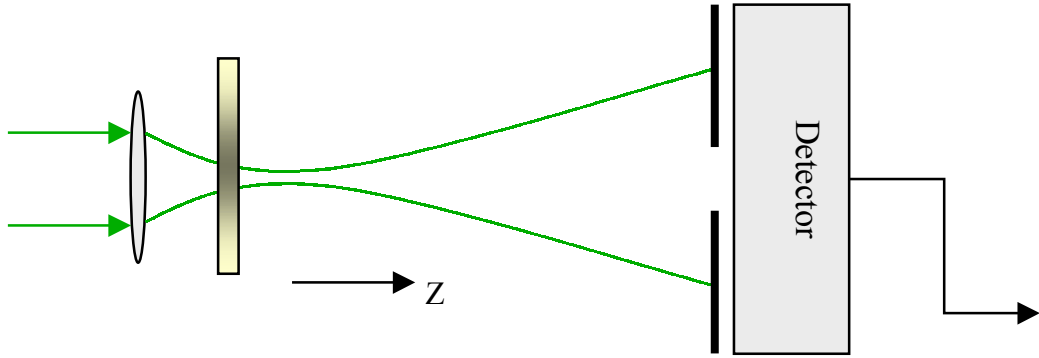


Figure 13

